PHILOSOPHICAL TRANSACTIONS OF THE ROYAL SOCIETY A MATHEMATICAL, PHYSICAL & ENGINEERING SCIENCES

Kinematic Dynamos and the Earth's Magnetic Field

C. L. Pekeris, Y. Accad and B. Shkoller

Phil. Trans. R. Soc. Lond. A 1973 **275**, 425-461
doi: 10.1098/rsta.1973.0111

KINEMATIC DYNAMOS AND THE EARTH'S MAGNETIC FIELD

By C. L. PEKERIS, Y. ACCAD and B. SHKOLLER
Department of Applied Mathematics, The Weizmann Institute, Rehovot, Israel

(*Communicated by Sir Edward Bullard, F.R.S. – Received* 11 *April* 1973)

CONTENTS

The Bullard–Gellman formalism is applied to investigate the existence of convergent solutions for steady kinematic dynamos. It is found that the solutions for the Bullard–Gellman dynamo, as well as for Lilley's modification of it, do not converge. Convergent solutions have been found for a class of spherical convective cells which would be stationary in a perfect fluid in the absence of rotation and of the magnetic field. By calibrating the theoretical magnetic dipole so as to fit the observed value at the Earth's surface, one can find a dynamo in the above class which also matches the observed equatorial magnetic dipoles. There is a dynamo S_4^{2c} which has a rate of total ohmic dissipation of only 1.8×10^{16} erg s^{-1} for an assumed electrical conductivity of 3×10^{-6} e.m.u.† This is one thousandth the rate of tidal dissipation, and one hundred thousandth the rate of heat outflow from the surface of the Earth. The required velocities are of the order of 10^{-3} cm s^{-1}, and the average magnetic energy density is 4 erg cm^{-3}. The internal structure of the magnetic field in this model shows a dynamo mechanism situated in the outer part of the liquid core and is thus insensitive to possible rigidity of the material in the 'inner core'.

1. Introduction

This investigation is concerned with the dynamo theory of the origin of the Earth's magnetic field, proposed by Larmor (1919). Larmor's idea that the field is produced through self-induction by convection currents which are assumed to exist in the conducting liquid core of the Earth was put into question by Cowling (1934), who proved that a magnetic field which has an axis of symmetry cannot be self-maintained. The theory of the self-exciting dynamo was revived by Elsasser (1946), and later Bullard & Gellman (1954) made the first study of a model for a self-

† 1 joule = 10^7 erg; 1 e.m.u. = $10^9 \Omega^{-1}$ cm^{-1}.

 [Published 15 November 1973

exciting stationary spherical dynamo. Bullard & Gellman restricted themselves to the case of the *kinematic dynamo*, in which the convection currents are assumed to be given and to be maintained without change. In the kinematic dynamo one disregards the hydrodynamic equation

$$\partial \boldsymbol{U}/\partial t + (\boldsymbol{U}.\mathrm{grad})\ \boldsymbol{U} + 2\boldsymbol{\Omega} \times \boldsymbol{U} = -\frac{1}{\rho}\mathrm{grad}\,(p+\Phi) - \frac{1}{4\pi\rho}(\boldsymbol{H} \times \mathrm{curl}\,\boldsymbol{H}) + \nu\nabla^2\boldsymbol{U}, \tag{1}$$

and investigates whether, for a given velocity field $\boldsymbol{U}$, the induction equation

$$\partial \boldsymbol{H}/\partial t = \lambda\nabla^2\boldsymbol{H} + \mathrm{curl}\,(\boldsymbol{U} \times \boldsymbol{H}) \tag{2}$$

possesses a sourceless solution which includes a component dipole field and meets the boundary conditions. Here $\boldsymbol{H}$ denotes the magnetic field, $\lambda = \frac{1}{4}\pi k$, k denoting the electrical conductivity, $\boldsymbol{\Omega}$ is the rotation vector of the Earth, p the pressure, ρ the density, Φ the potential of the gravitational and centrifugal forces, and ν the kinematic viscosity. The condition that the field produced by the dynamo should include a dipole component is required, of course, because the Earth's magnetic field is predominantly a dipole, to within 20 %. The induction equation (2) follows from Maxwell's equations

$$\mathrm{curl}\,\boldsymbol{H} = 4\pi\boldsymbol{j}, \tag{3}$$

$$\boldsymbol{j} = k(\boldsymbol{E} + \boldsymbol{U} \times \boldsymbol{H}), \tag{4}$$

$$\mathrm{curl}\,\boldsymbol{E} = -\partial \boldsymbol{H}/\partial t, \tag{5}$$

$$\mathrm{div}\,\boldsymbol{H} = 0, \tag{6}$$

$$\mathrm{div}\,\boldsymbol{E} = 4\pi q c^2, \tag{7}$$

upon elimination of the electric vector $\boldsymbol{E}$ from (3), (4) and (5). Here q denotes the electric charge density, and c the velocity of light. In (4) we have omitted terms which are of the order of U^2/c^2 (Bullard 1955).

If we take the radius of the core b as the unit of length, $4\pi kb^2$ as the unit of time, and measure velocities in units of U_0, then equation (2) takes the form

$$\partial \boldsymbol{H}/\partial t = \nabla^2\boldsymbol{H} + R\,\mathrm{curl}\,(\boldsymbol{U} \times \boldsymbol{H}), \tag{8}$$

with the magnetic Reynolds number R defined by

$$R = 4\pi kbU_0. \tag{9}$$

Following the Bullard–Gellman formalism (Bullard & Gellman 1954), we represent the solution $\boldsymbol{H}^i$ of (6) for the *interior* of the core by

$$H_r^i = \sum_\beta \frac{\beta(\beta+1)}{r^2} S_\beta(r)\, Y_\beta, \tag{10}$$

$$H_\theta^i = \sum_\beta \left[\frac{\dot{S}_\beta(r)}{r}\frac{\partial Y_\beta}{\partial\theta} + \frac{T_\beta(r)}{r\sin\theta}\frac{\partial Y_\beta}{\partial\phi}\right], \tag{11}$$

$$H_\phi^i = \sum_\beta \left[\frac{\dot{S}_\beta(r)}{r\sin\theta}\frac{\partial Y_\beta}{\partial\phi} - \frac{T_\beta(r)}{r}\frac{\partial Y_\beta}{\partial\theta}\right], \tag{12}$$

where

$$Y_\beta = P_\beta^{m_\beta}(\cos\theta)\,[\cos m_\beta\phi, \sin m_\beta\phi], \tag{13}$$

the dot denoting differentiation with respect to r and the summation on β implying also

summation over m_β. The functions S_β represent the *poloidal* components of the field and T_β the *toroidal*. Outside the core, the field $\boldsymbol{H}^e$ is represented by

$$H_r^e = \sum_\beta \beta(\beta+1)\, S_\beta(1) \left(\frac{b}{r}\right)^{\beta+2} Y_\beta, \tag{14}$$

$$H_\theta^e = -\sum_\beta \beta S_\beta(1) \left(\frac{b}{r}\right)^{\beta+2} \frac{\partial Y_\beta}{\partial \theta}, \tag{15}$$

$$H_\phi^e = -\sum_\beta \beta S_\beta(1) \left(\frac{b}{r}\right)^{\beta+2} \frac{1}{\sin\theta} \frac{\partial Y_\beta}{\partial \phi}. \tag{16}$$

The continuity conditions on $\boldsymbol{H}$ at the surface of the core ($r = 1$) require that

$$\dot{S}_\beta(1) + \beta S_\beta(1) = 0, \quad T_\beta(1) = 0. \tag{17}$$

In the case of the *stationary* kinematic dynamo, Bullard & Gellman (1954) showed that the induction equation

$$\nabla^2 \boldsymbol{H} + R \operatorname{curl}(\boldsymbol{U} \times \boldsymbol{H}) = 0, \tag{18}$$

subject to the boundary condition (17) and to the condition of finiteness at the origin, leads to an eigenvalue problem for the magnetic Reynolds number R defined in (9).

In the discussions of the dynamo theory so far, the liquid was assumed to be incompressible:

$$\operatorname{div} \boldsymbol{U} = 0, \tag{19}$$

although this assumption is not essential (Pekeris 1971). With (19), an appropriate representation of the velocity field $\boldsymbol{U}$ is, again,

$$u_r = \sum_\alpha \frac{\alpha(\alpha+1)}{r^2} S_\alpha(r)\, Y_\alpha, \tag{20}$$

$$u_\theta = \sum_\alpha \left[\frac{\dot{S}_\alpha(r)}{r} \frac{\partial Y_\alpha}{\partial \theta} + \frac{T_\alpha(r)}{r \sin\theta} \frac{\partial Y_\alpha}{\partial \phi}\right], \tag{21}$$

$$u_\phi = \sum_\alpha \left[\frac{\dot{S}_\alpha(r)}{r \sin\theta} \frac{\partial Y_\alpha}{\partial \phi} - \frac{T_\alpha(r)}{r} \frac{\partial Y_\alpha}{\partial \theta}\right]. \tag{22}$$

Using the representations (10) to (12) and (20) to (22) in the induction equation (18), we are led by the Bullard–Gellman formalism to a series of simultaneous ordinary differential equations of the form (Bullard & Gellman 1954)

$$r^2 \ddot{S}_\gamma - \gamma(\gamma+1)\, S_\gamma = R \sum_\alpha \sum_\beta F_\gamma(S_\alpha, S_\beta, T_\alpha, T_\beta), \tag{23}$$

$$r^2 \ddot{T}_\gamma - \gamma(\gamma+1) T_\gamma = R \sum_\alpha \sum_\beta G_\gamma(S_\alpha, S_\beta, T_\alpha, T_\beta). \tag{24}$$

Here F_γ and G_γ are linear functions of the unknowns and of their first and second derivatives, with coefficients depending on the velocity functions S_α and T_α.

2. The Bullard–Gellman dynamo

The specific form of the basic differential equations (23) and (24) depends on the assumed velocity field (20) to (22), because of certain 'selection rules' (Elsasser 1946) which result from

the coupling term $\boldsymbol{U}\times\boldsymbol{H}$ in (18). The most thoroughly investigated case is the Bullard–Gellman (1954) dynamo, in which the convection is represented by

$$u_r = \frac{6}{r^2} Q_S(r)\, P_2^2(\cos\theta)\cos 2\phi, \tag{25}$$

$$u_\theta = \frac{\dot{Q}_S(r)}{r}\,\frac{\partial}{\partial\theta} P_2^2(\cos\theta)\cos 2\phi, \tag{26}$$

$$u_\phi = \frac{1}{r\sin\theta}\,\dot{Q}_S(r)\, P_2^2(\cos\theta)\,\frac{\partial}{\partial\phi}\cos 2\phi - \frac{Q_T(r)}{r}\,\frac{\partial P_1(\cos\theta)}{\partial\theta}, \tag{27}$$

$$Q_S = r^3(1-r)^2, \quad Q_T = \epsilon r^2(1-r). \tag{28}$$

It is composed of a poloidal component S_2^{2c} (the superscript 2c referring to the $\cos 2\phi$ factor) and of a toroidal component T_1. A test as to whether the Bullard–Gellman convection cell (25) to (28) can act as a self-exciting dynamo is that the eigenvalue R of (18) should converge as the number of terms in the expansions (10) to (12) is increased. The original work of Bullard & Gellman was followed by an investigation of Gibson & Roberts (1969),† and subsequently by Lilley (1970). We have repeated the calculations, and the results are summarized in table 1. We have used finite differences, with an interval h of 0.01 or less. The starred values were also obtained by expanding the unknown functions into series of spherical Bessel functions. The latter are solutions of the homogeneous equations (23) and (24). We found this expansion to be quite feasible, thus offering a convenient method of treating the nonstationary dynamo (Elsasser 1946). The values quoted from Lilley are those derived with his finest subdivision.

Clearly the eigenvalues shown in table 1 do not show a tendency towards convergence.‡ Hence, none of the four models investigated can be considered to have been proven capable of maintaining a stationary self-exciting dynamo.

3. Stationary spherical vortices

In looking for other convective cells to be tested as to their capability of acting as self-exciting dynamos, we shall adopt the criterion that the *motion be stationary in the case of a perfect fluid* (Pekeris 1972). This means that we seek solutions of the hydrodynamic equation (1) when it is truncated to the form

$$(\boldsymbol{U}.\mathrm{grad})\,\boldsymbol{U} = -(1/\rho)\,\mathrm{grad}\,(p+\Phi). \tag{29}$$

In the case of an incompressible fluid, spherical vortices which are solutions of (29) exist (Pekeris 1972). The class discussed so far is characterized by a single spherical harmonic Y_α in (20) to (22), with

$$S_\alpha(r) = x j_\alpha(x), \quad x = \lambda r, \tag{30}$$

$$T_\alpha(r) = \lambda S_\alpha(r), \tag{31}$$

where $j_\alpha(x)$ is the spherical Bessel function of order α:

$$j_n(x) = (\pi/2x)^{\frac{1}{2}} J_{n+\frac{1}{2}}(x). \tag{32}$$

† The coefficient $\frac{11}{5}^2$ appearing in the equation for S_5^{2s} on p. 583 of Gibson & Roberts should be replaced by $\frac{16}{5}$.

‡ The non-convergence of the Lilley model was found independently by Roberts (1972) and Gubbins (1972).

PHILOSOPHICAL TRANSACTIONS OF THE ROYAL SOCIETY A MATHEMATICAL, PHYSICAL & ENGINEERING SCIENCES

TABLE 1. EIGENVALUES R FOR THE BULLARD–GELLMAN MODEL

n denotes the maximum spherical harmonic order included, N the total number of unknown functions. GR = Gibson & Roberts (1969), L = Lilley (1970), PAS = present authors.

model I:	$Q_S^{2c}(r) = r^3(1-r)^2$	$Q_T(r) = 5r^2(1-r)$
model II:	$Q_S^{2c}(r) = r^3(1-r)^2$	$Q_T(r) = 10r^2(1-r)$
model III:	$Q_S^{2c}(r) = r^3(1-r^2)^2$	$Q_T(r) = 5r^2(1-r^2)$
model IV:	$Q_S^{2c}(r) = r^3(1-r^2)^2$	$Q_T(r) = 10r^2(1-r^2)$
	$Q_S^{2s}(r) = 1.6r^3(1-4r^2)^2$	$0 \leqslant r \leqslant 0.5$
	$= 0$	$0.5 \leqslant r \leqslant 1$

n	...	2			3			4			5		
N	...	4			7			12			17		
authors		GR	L	PAS	GR	L	PAS	GR	L	PAS	GR	L	PAS
model I		66.5	64.4	66.460*	83.1	78.5	83.207*	75.9	94.3	95.834	143.2	—	1369.2
II		—	50.4	53.465	—	70.2	80.934	—	75.0	80.913	—	102.3	131.696
III		—	—	41.111	—	—	41.843	—	—	46.512	—	—	129.225
IV		—	25.97	26.886	—	39.91	39.198	—	17.76	33.692	—	21.28	171.20

The vanishing of the radial component of velocity u_r at the surface of the core requires, by (20) and (30), that λ_ν be a root of the equation

$$j_\alpha(\lambda_\nu) = 0. \tag{33}$$

These solutions are Beltrami flows, which, for $n > 1$, satisfy the equation

$$\text{curl } \boldsymbol{U} = \lambda \boldsymbol{U}. \tag{34}$$

They represent spiral flows, whose 'helicity' (Moffat 1969) has the sign of λ.

In the liquid core of the Earth the Coriolis force $-2\boldsymbol{\Omega} \times \boldsymbol{U}$ and the magnetic braking force $-\boldsymbol{H} \times \text{curl } \boldsymbol{H}$ are, of course, not negligibly small. Our aim was first to ascertain whether a spherical vortex which is stationary in an inviscid liquid can produce a self-maintaining dynamo. Should that prove feasible, then, as a next step, we would consider the modifications introduced by the rotation and by the magnetic braking forces.

In the definition of the magnetic Reynolds number R in (9) it was implied that the velocity field $\boldsymbol{U}$ is represented by

$$\boldsymbol{U} = U_0 \boldsymbol{F}(r/b), \tag{35}$$

where U_0 represents the amplitude of the velocity, and the function $\boldsymbol{F}$ is of the order of unity. Accordingly, we shall apply a normalizing factor to the velocity components (20) to (22) such that

$$\overline{u^2} = \int_0^{2\pi} \mathrm{d}\phi \int_0^{\pi} \sin\theta \, \mathrm{d}\theta \int_0^1 r^2 \, \mathrm{d}r \, (u_r^2 + u_\theta^2 + u_\phi^2) = \tfrac{4}{3}\pi. \tag{36}$$

Writing n for α, we put

$$u_r = \frac{1}{A} \frac{n(n+1)}{r^2} S_n Y_n, \tag{37}$$

$$u_\theta = \frac{1}{Ar}\left[\dot{S}_n \frac{\partial Y_n}{\partial \theta} + \frac{T_n}{\sin\theta} \frac{\partial Y_n}{\partial \phi}\right], \tag{38}$$

$$u_\phi = \frac{1}{Ar}\left[\frac{\dot{S}_n}{\sin\theta} \frac{\partial Y_n}{\partial \phi} - T_n \frac{\partial Y_n}{\partial \theta}\right], \tag{39}$$

where $T_n = \lambda S_n$ and

$$\ddot{S}_n + \left[\lambda^2 - \frac{n(n+1)}{r^2}\right] S_n = 0. \tag{40}$$

Substituting in (36), we get

$$A^2\overline{u^2} = N_n \int_0^1 \mathrm{d}r \left[\frac{n(n+1)}{r^2} S_n^2 + \dot{S}_n^2 + T_n^2\right] = 2\lambda^2 N_n \int_0^1 S_n^2 \, \mathrm{d}r = \tfrac{4}{3}\pi A^2, \tag{41}$$

since, by (40), we have

$$\int_0^1 \mathrm{d}r \left[\frac{n(n+1)}{r^2} S_n^2 + \dot{S}_n^2\right] = \lambda^2 \int_0^1 S_n^2 \, \mathrm{d}r. \tag{42}$$

Equation (42) implies that in our convective cell there is equipartition of kinetic energy between the poloidal and toroidal components of the velocities (Chandrasekhar & Kendall 1957). In (41),

$$N_n = \frac{2\pi n(n+1)\,(n+m)!}{(2n+1)\,(n-m)!} \quad (m \neq 0), \tag{43}$$

$$N_n = \frac{4\pi n(n+1)}{2n+1} \quad (m = 0). \tag{44}$$

Now $$\int_0^1 S_n^2 \,\mathrm{d}r = (\tfrac{1}{2}\lambda\pi)\int_0^1 r\,\mathrm{d}r J_{n+\frac{1}{2}}^2(\lambda r) = (\tfrac{1}{4}\lambda\pi)\, J_{n+\frac{3}{2}}^2(\lambda); \tag{45}$$

hence, by (41), $$A_\nu = (\tfrac{3}{8}N_n)^{\frac{1}{2}}\lambda_\nu^{\frac{3}{2}}|J_{n+\frac{3}{2}}(\lambda_\nu)|. \tag{46}$$

4. The S_2^{2c} convective cell

The convective cell which we studied in the first instance is of the type S_2^{2c}, with

$$S_n = Q_n(r)\, Y_n(\theta,\phi),$$

$$Y_n = P_2^2(\cos\theta)\cos 2\phi = 3\sin^2\theta\cos 2\phi, \tag{47}$$

and $$Q_n(r) = \sqrt{(\tfrac{1}{2}\pi x)}\, J_{\frac{5}{2}}(x) = \left[\left(\frac{3}{x^2}-1\right)\sin x - \frac{3}{x}\cos x\right], \quad x = \lambda r. \tag{48}$$

In the computations we evaluated eigenvalues R' on the assumption that the factor A in (37) to (39) is unity. Hence the eigenvalue R defined in (9) is given by

$$R = AR'. \tag{49}$$

By (46) we have $$A_\nu = (\tfrac{108}{5}\pi)^{\frac{1}{2}}\lambda_\nu^{\frac{3}{2}}|J_{\frac{7}{2}}(\lambda_\nu)|, \tag{50}$$

which varies with the root λ_ν of $$J_{\frac{5}{2}}(\lambda_\nu) = 0. \tag{51}$$

In the general case when Y_n in (37) to (39) is given by

$$Y_n = \sum_{m=0}^{m=n}(A_n^m\cos m\phi + B_n^m\sin m\phi)\, P_n^m(\cos\theta), \tag{52}$$

A_ν is determined from

$$A_\nu = \lambda_\nu^{\frac{3}{2}}|J_{n+\frac{3}{2}}(\lambda_\nu)|\left\{\frac{3}{8}\sum_{m=0}^{m=n} N_n^m[(A_n^m)^2+(B_n^m)^2]\right\}^{\frac{1}{2}}. \tag{53}$$

Using the representation (37) to (39), with (47) and (48), we solved the Bullard–Gellman system of equations (23) and (24) by finite differences. The integration interval $0 \leqslant r \leqslant 1$ was divided into equal steps h of 0.01, and the determinant of the resulting equations (23) and (24) was solved for the eigenvalue R. Spot-checks were carried out by taking $h = 0.005$. *The eigenvalue R did converge*, as is shown in table 2 for the case of the third root λ_3 of (51). A more stringent test of convergence is the magnetic energy integral I defined in (A 10), and even more so the ohmic dissipation integral J of (A 17). In order to obtain manifestly convergent results for the latter integrals one has to refine the eigenvalues to many more decimals than are given in table 2, since slight errors in the eigenvectors are amplified by the huge factors N_β; in the case of $N = 98$, for instance, $N_{13}^{12} = 6.57\times 10^{26}$.

The values in table 2 show an oscillation with a damped amplitude. The extrapolation was made by fitting the data to

$$R_n = R_\infty + A\,\mathrm{e}^{-\alpha x}\cos\beta x + B\,\mathrm{e}^{-\alpha x}\sin\beta x. \tag{54}$$

The functions were normalized so that

$$S_1^0(1) = -1. \tag{55}$$

The minus sign was chosen because the dipole magnetic field at the north pole, which is proportional to $S_1^0(1)$, is downward. The degree of convergence of the poloidal dipole field $S_1^0(r)$ is shown in figure 1, as the number N of the functions included in the expansion (10) to (12)

PHILOSOPHICAL TRANSACTIONS OF THE ROYAL SOCIETY A MATHEMATICAL, PHYSICAL & ENGINEERING SCIENCES

TABLE 2. THE EIGENVALUES R_3 FOR THE THIRD MODE OF THE S_2^{2c} CONVECTIVE CELL

$\lambda_3 = 12.322941$ is the third root of (51); n denotes the maximum order of spherical harmonics retained in (10) to (12), N the total number of unknown functions in (23) and (24); I is the magnetic energy integral (A 10), and J the dissipation integral (A 17). I_S and I_T are the poloidal and toroidal components of I. The scaling factor A_3 in (50) is 80.191.

n	6	7	8	9	10	11	12	13	∞
N	24	32	40	50	60	72	84	98	—
R_3'	0.4213	0.3410	0.3510	0.3783	0.3707	0.3623	0.3638	0.3662	0.3655
$R_3 = A_3 R_3'$	33.78	27.35	28.15	30.34	29.73	29.05	29.17	29.37	29.31
I_S	204.4	183.7	186.6	196.1	192.6	190.4	191.0	191.8	191.6
I_T	330.6	361.0	355.7	343.3	344.3	348.0	347.6	346.4	346.8
J_S	32 762	27 050	28 499	32 122	31 328	30 601	30 862	31 211	31 040
J_T	21 644	22 541	22 293	21 714	21 619	21 720	21 693	21 618	21 680
I	535.0	544.7	542.3	539.4	536.9	538.4	538.6	538.2	538.4
J	54 406	49 591	50 792	53 836	52 947	52 321	52 555	52 829	52 720

varies from 50 to 98. The distribution of the toroidal field $T_1^0(r)$ is shown in figure 2. Although $T_1^0(r)$ is greater by an order of magnitude than S_1^0, the resulting components of the dipole field

$$H_{1r}^0 = \frac{2}{r^2} S_1^0(r) \cos\theta, \quad H_{1\theta}^0 = -\frac{\dot{S}_1^0(r)}{r} \sin\theta, \quad H_{1\phi}^0 = \frac{T_1^0(r)}{r} \sin\theta, \tag{56}$$

are of comparable magnitude, as is shown in figure 3. However, T_1^0 contributes 54 % of the total magnetic energy integral I of (A 10) shown in table 2, while the dipole field contributes 18 %. The higher order functions converge at a slower rate with increasing N, as is shown in figures 4 and 5.

The rate of convergence of the solution is shown in figure 6, where we have plotted the integrals $I(S_n^m)$ representing the contributions of the poloidal field components S_n^m to the magnetic energy

$$I(S_n^m) = \frac{1}{\pi} N_n^m \int_0^1 [n(n+1)\,(S_n^m/r)^2 + (\dot{S}_n^m)^2]\,\mathrm{d}r. \tag{57}$$

In each S_n^m group the biggest contribution comes from the terms S_n^n or S_n^{n-1}. Figure 7 shows the contributions $I(T_n^m)$ of the toroidal field components T_n^m to the magnetic energy.

The *magnetic energy density* e_{M} is obtained from (A 9) by dividing E_{M} by the volume of the core

$$e_{\mathrm{M}} = (\tfrac{3}{32}\pi) I \Gamma^2, \tag{58}$$

where

$$\Gamma = 0.3043(a/b)^3 = 1.88G. \tag{59}$$

The scaling factor Γ arises from the fact that the observed spherical harmonic coefficient of the dipole field (Cain, Daniels & Hendricks 1965)

$$g_1^0 = -0.3043G \tag{60}$$

is related, through (10) and (55), to $S_1^0(1)$ by

$$2(a/b)^3 g_1^0 = 2S_1^0(1)\,\Gamma. \tag{61}$$

Using the value of $I = 538.4$, we deduce from (58) that the *magnetic energy density is* 57 erg cm^{-3}. With a density of about 11 g cm^{-3} for the core, it would take a velocity of about 3 cm s^{-1} to produce an equal kinetic energy density. On the other hand, the eigenvalue of $R = 29.31$ yields, by (9), a value of 0.0022 cm s^{-1} for the velocity scale U_0 of the convection. Here we have assumed that the electrical conductivity $\kappa = 3 \times 10^{-6}$ e.m.u. It follows that the magnetic energy density is greater by about a factor of 10^6 than the kinetic energy density in the convective cell.

Taking the value of $J = 5.27 \times 10^4$ we get, from (A 16), for the rate of total joule heat dissipation,

$$D = 4.3 \times 10^{17} \text{ erg s}^{-1}. \tag{62}$$

This is small in comparison with the rate of tidal dissipation of 1.5×10^{19} erg s^{-1} (Jeffreys 1970), or with the rate of heat flux from the Earth of 95×10^{19} erg s^{-1}.

5. Matching the equatorial magnetic dipole components

Since the induction equation (2) is linear in $\boldsymbol{H}$, its amplitude is calibrated by fitting $S_1^0(1)$ to the value of $-0.3043G$ for the dipole term g_1^0 in the expansion of the observed external magnetic potential W:

$$W = a \sum_{n=1}^{\infty} \sum_{m=0}^{n} (a/r)^{n+1} \lambda_n^m (g_n^m \cos m\phi + h_n^m \sin m\phi)\, P_n^m(\cos\theta), \tag{63}$$

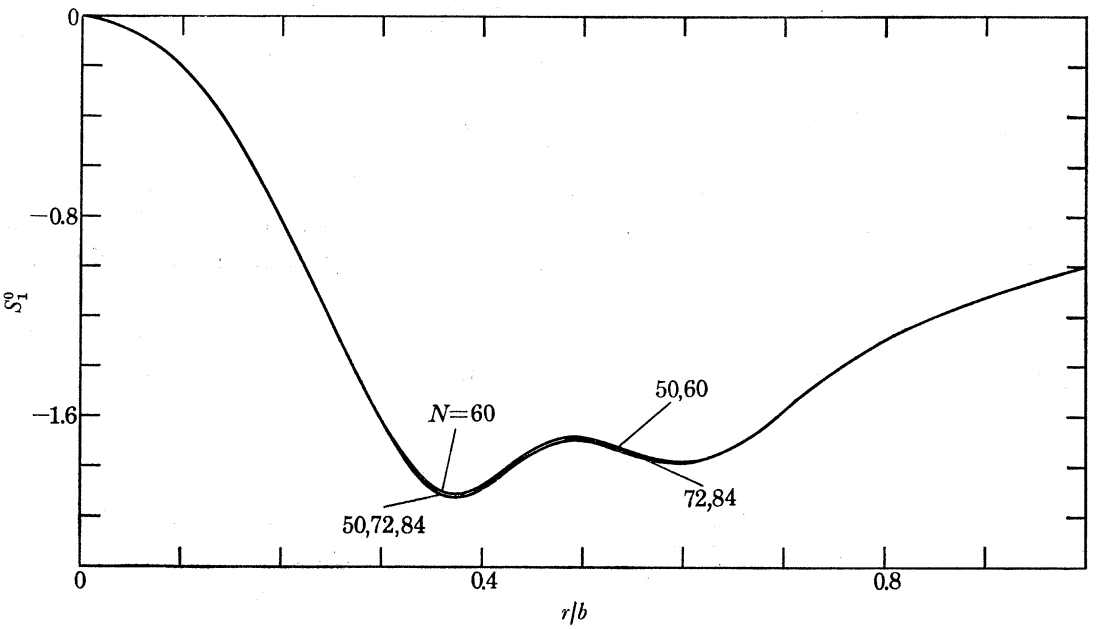

FIGURE 1. Distribution of the dipole field S_1^0 inside the core. S_2^{2c} convective cell.

$$S_\alpha = Q(r)\,P_2^2(\cos\theta)\cos 2\phi \qquad T_\alpha = \lambda Q(r)\,P_2^2(\cos\theta)\cos 2\phi,$$
$$Q(r) = \sqrt{(\tfrac{1}{2}\pi\lambda r)}\,J_{\frac{5}{2}}(\lambda r), \qquad \lambda = \lambda_3 = 12.32294.$$

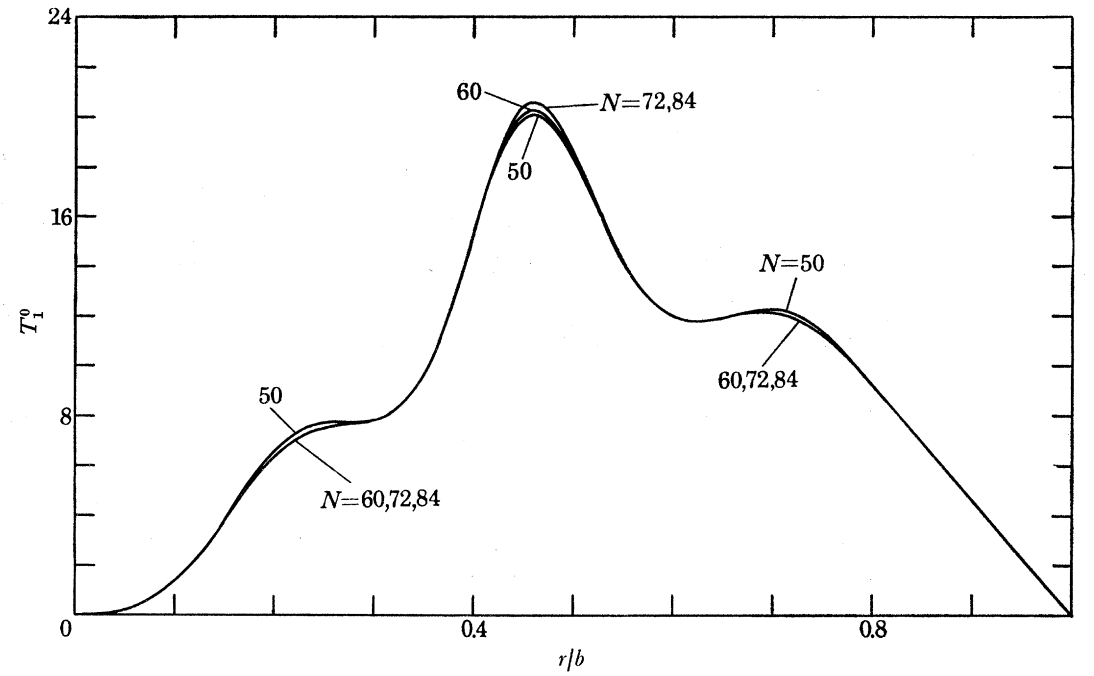

FIGURE 2. Distribution of the toroidal field T_1^0 inside the core. S_2^{2c} convective cell.

$$S_\alpha = Q(r)\,P_2^2(\cos\theta)\cos 2\phi, \qquad T_\alpha = \lambda Q(r)\,P_2^2(\cos\theta)\cos 2\phi,$$
$$Q(r) = \sqrt{(\tfrac{1}{2}\pi\lambda r)}\,J_{\frac{5}{2}}(\lambda r), \qquad \lambda = \lambda_3 = 12.32294.$$

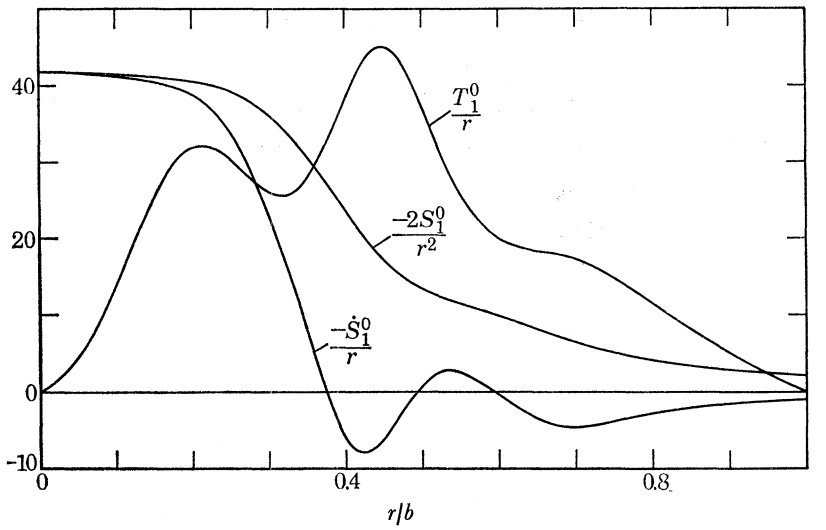

FIGURE 3. The amplitudes of the components of the dipole field in equation (56) for the S_2^{2c} convective cell. $\lambda = \lambda_3 = 12.32294$.

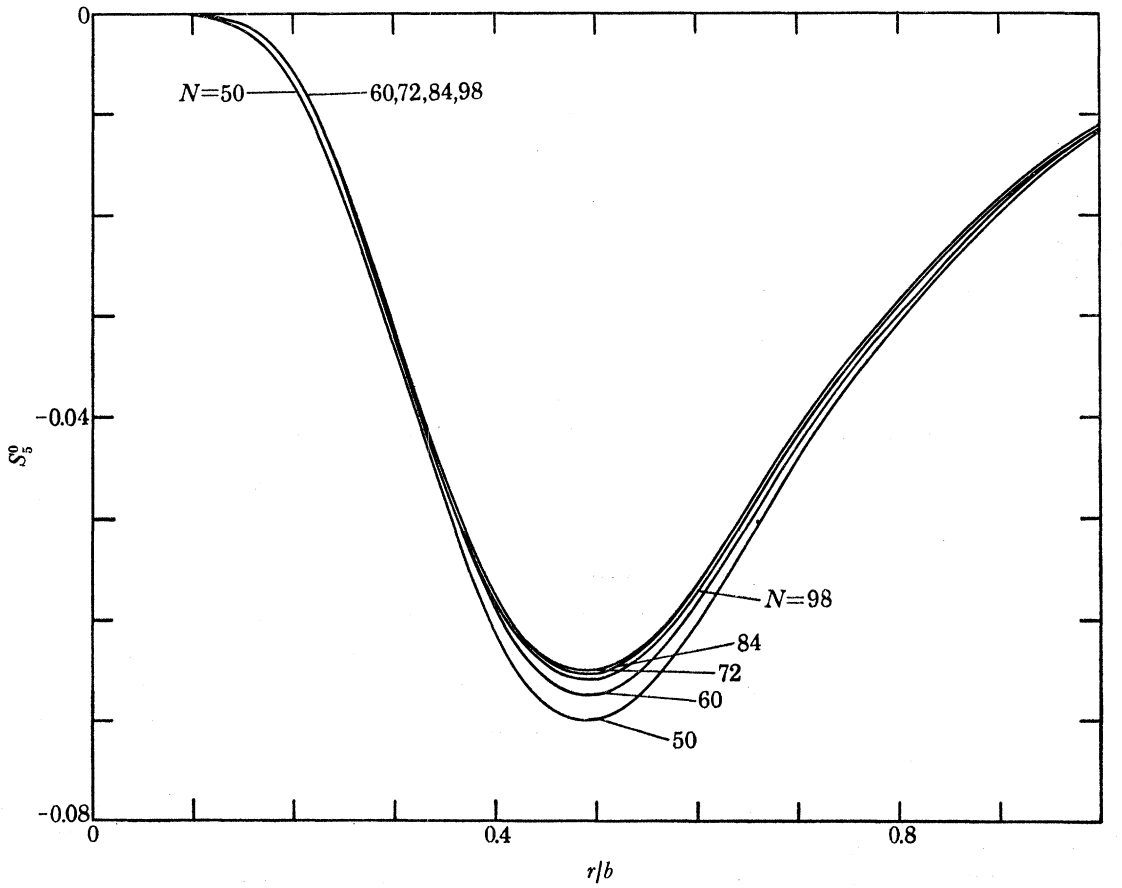

FIGURE 4. Distribution of the poloidal field S_5^0 inside the core. S_2^{2c} convective cell. $\lambda = \lambda_3 = 12.32294$.

PHILOSOPHICAL TRANSACTIONS OF THE ROYAL SOCIETY A MATHEMATICAL, PHYSICAL & ENGINEERING SCIENCES

where
$$\lambda_n^m = [2(n-m)!/(n+m)!]^{\frac{1}{2}}, \quad m > 0,$$
$$= 1, \quad m = 0. \tag{64}$$

By evaluating $\boldsymbol{H} = -\text{grad}\, W$ and equating coefficients with the corresponding terms in (14) to (16), we obtain for the theoretical values of the non-dipole harmonic coefficients:

$$(\lambda_n^m g_n^m)_{\text{th}} = 1.878n(b/a)^{n+2} S_n^{mc}(1), \tag{65}$$
$$(\lambda_n^m h_n^m)_{\text{th}} = 1.878n(b/a)^{n+2} S_n^{ms}(1). \tag{66}$$

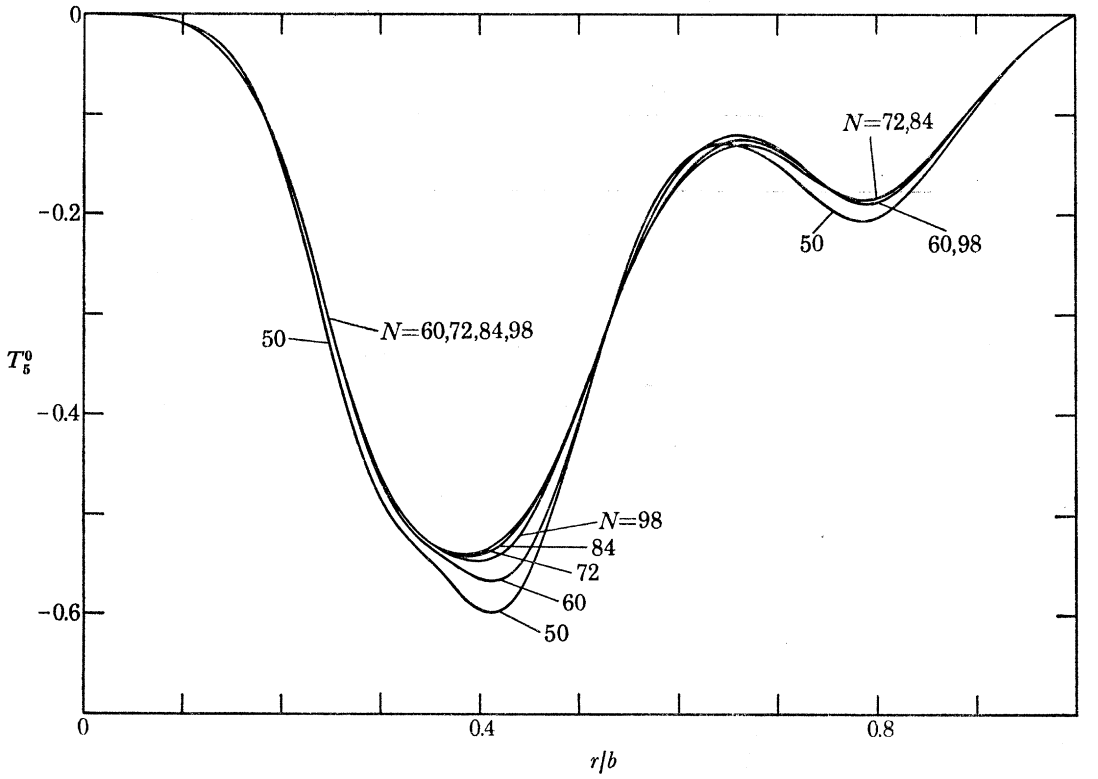

FIGURE 5. Distribution of the toroidal field T_5^0 inside the core. S_2^{2c} convective cell. $\lambda = \lambda_3 = 12.32294$.

Of these, the biggest observed terms are

$$g_1^1 = -0.0217G, \quad h_1^1 = 0.0576G, \tag{67}$$

which represent the deviation of the magnetic axis from the axis of rotation, or the *equatorial components of the magnetic dipole*. For the S_2^{2c} convective cell the theoretical equatorial dipole terms are strictly zero as a consequence of the selection rules. The first non-vanishing theoretical non-dipole term is $(h_2^2)_{\text{th}} = 0.0315G$ which, along with the other higher order harmonic coefficients, is of the right order of magnitude.

By adding an S_2^{1c} term to the S_2^{2c} surface spherical harmonic, we can generate a non-vanishing g_1^1 component, and similarly the combination $(S_2^{2c} + \epsilon S_2^{1s})$ generates an h_1^1 term in the magnetic field. The observed equatorial dipole terms in (67) can be matched approximately if instead of S_2^{2c} we choose an angular factor

$$Y_2 = (S_2^{2c} - 0.144 S_2^{1c} - 0.400 S_2^{1s})$$
$$= 3(\sin^2\theta \cos 2\phi - 0.144 \cos\theta \sin\theta \cos\phi - 0.400 \cos\theta \sin\theta \sin\phi). \tag{68}$$

The resulting theoretical surface harmonic coefficients for the magnetic field are given in table 3. We see that the equatorial dipole terms are approximately matched, while the theoretical higher order harmonic coefficients are of the right order of magnitude.

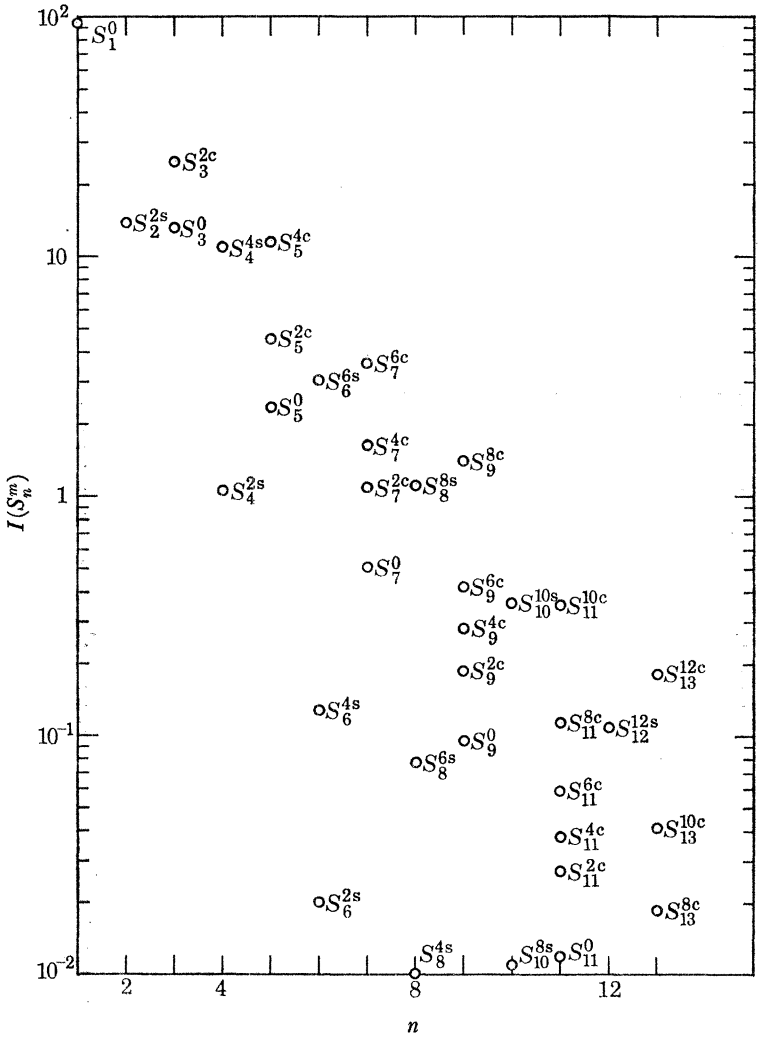

FIGURE 6. The magnetic energy integral $I(S_n^m)$ for the poloidal field components S_n^m.

$$I(S_n^m) = \frac{1}{\pi} N_n^m \int_0^1 [n(n+1)\,(S_n^m/r)^2 + (\dot{S}_n^m)^2]\,\mathrm{d}r.$$

S_2^{2c} convective cell. $\lambda = \lambda_3 = 12.32294$.

The combination (68) has a physical basis. If we take a rectangular coordinate system

$$x = \sin\theta\cos\phi, \quad y = \sin\theta\sin\phi, \quad z = \cos\theta, \tag{69}$$

then Y_2 in (68) becomes

$$\tfrac{1}{3}Y_2 = (x^2 - y^2 - 0.144xz - 0.400yz) \tag{70}$$

$$= 1.00526x'^2 - 1.0386y'^2 + 0.0333z'^2,$$

where we have effected an orthogonal transformation to a rectangular coordinate system

(x', y', z') passing through the principal axes of the surface (70). The transformation is given by

	x	y	z
x'	0.9969	0.00775	−0.0777
y'	0.00670	0.9818	0.1898
z'	0.0729	−0.1895	0.9792

The coordinates of the z'-axis on the unit sphere are given by

$$x = 0.0729, \quad y = -0.1895, \quad z = 0.9792. \tag{71}$$

This corresponds to

$$\theta = 11.7°, \quad \phi = -69°, \tag{72}$$

which are the coordinates of the magnetic axis of the Earth. In the magnetic spherical coordinate system $(x', y, ' z')$, Y_2 of (68) is given by

$$Y_2 = 1.0219(S_2^{2c})' + 0.10004(S_2^0)'. \tag{73}$$

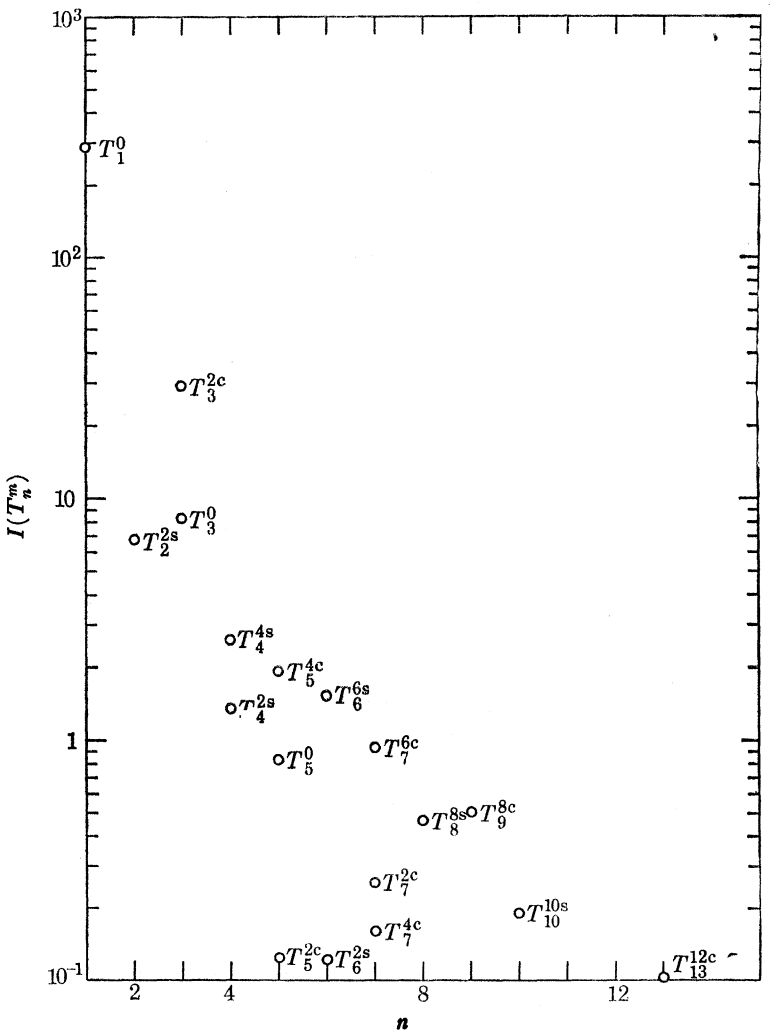

FIGURE 7. The magnetic energy integral $I(T_n^m)$ of the toroidal component T_n^m of the field.

$$I(T_n^m) = \frac{1}{\pi} N_n^m \int_0^1 (T_n^m)^2 \, dr; \; \lambda = \lambda_3 = 12.32294.$$

The $S_2^{1c}(r)$ and $S_2^{1s}(r)$ functions obtained from the solution of the induction equation for the convective cell represented by (68) are proportional to $S_1^0(r)$ throughout the core, indicating a projection of a magnetic dipole vector on to the axis of rotation. The magnetic Reynolds number R and the dissipation integral J are close to the values given in table 2 for the S_2^{2c} model.

The surface harmonic Y_2 in (68), which was adjusted to match the observed equatorial magnetic dipole terms in the case of the third root of (51), also applies to all the other roots. As seen from table 4 below, the first mode has a rate of ohmic dissipation which is less than one-fourth of that of the third mode.

TABLE 3. SPHERICAL HARMONIC COEFFICIENTS FOR THE MAIN FIELD/10^{-4} G

$$W = a\sum_{n=1}^{\infty}\sum_{m=0}^{n}(a/r)^{n+1}(g_n^m\cos m\phi + h_n^m\sin m\phi)\,P_n^m(\cos\theta).$$

source	year	g_1^0	g_1^1	h_1^1	g_2^0	g_2^1	h_2^1	g_2^2	h_2^2
Erman & Petersen	1829	−3201	−284	601	−8	257	−4	−14	146
Gauss	1835	−3235	−311	625	51	292	12	−2	157
Adams, J. C.; Adams, W. G.	1845	−3219	−278	578	9	284	−10	4	135
Adams, J. C.; Adams, W. G.	1880	−3168	−243	603	−49	297	−75	61	149
Schmidt	1885	−3168	−222	595	−50	278	−71	65	149
Fritsche	1885	−3164	−241	591	−35	286	−75	68	142
Neumeyer & Petersen	1885	−3157	−248	603	−53	288	−75	65	146
Dyson & Furner	1922	−3095	−226	592	−89	299	−124	144	84
Jones & Melotte	1942	−3039	−218	555	−117	294	−150	157	51
Afanasieva	1945	−3032	−229	590	−125	288	−146	150	48
Vestine *et al.*	1945	−3057	−211	581	−127	296	−166	164	54
Finch & Leaton	1955	−3055	−227	590	−152	303	−190	158	24
Cain & Daniels	1940–62	−3043	−217	576	−155	300	−195	157	20
S_2^{2c}		−3043	0	0	0	0	0	0	315
$S_2^{2c}-0.144S_2^{1c}-0.400S_2^{1s}$		−3043	−227	589	−8	61	−23	0	315
$S_4^{2c}+0.026S_4^{3c}-0.017S_4^{3s}$		−3043	−121	577	87	−101	237	23	462

6. A KINEMATIC DYNAMO OF MINIMUM OHMIC DISSIPATION

In the preceding section we have demonstrated that a manifestly converging solution of the steady induction equation (18) exists for the case of the third mode of an S_2^{2c} convective spherical cell described in § 3. The representation of the solution for $\boldsymbol{H}$ included all spherical harmonics through order 13, making a total of 98 unknown functions, and the degree of convergence is exhibited in table 2 and in figures 1 to 7. We found that steady kinematic dynamos also exist for other cases of spherical convective cells belonging to the class discussed in § 3. In starting with the S_2^{2c} cell we were motivated by a conjecture that the dynamo might be driven by the tidal forces (Pekeris 1971) which have that angular form. The third mode was chosen because it appeared to converge most easily. Subsequent investigation showed that all the modes of the S_2^{2c} convective cell yield steady kinematic dynamos. The results are given in table 4. In the case of the first mode λ_1 we had to include all spherical harmonics through order 15 (128 unknown functions) before the solution visibly converged. The magnetic Reynolds number R decreases from a value of 99 for λ_1 to an asymptotic value of 26.4 for the higher order modes. The ohmic dissipation integral J increases monotonically with the increasing order ν of the mode, and so does the magnetic energy integral I. With $I = 111$ for the first mode, the magnetic energy density is 12 erg cm^{-3},

while the rate of total ohmic dissipation is 9.9×10^{16} erg s^{-1}. With $R = 99$, the velocity U_0 of convection required 0.0075 cm s^{-1}.

Since the ohmic dissipation for the first mode of the S_2^{2c} cell turned out to be less than for the third mode discussed previously, we looked for a convective cell of even lower dissipation. We found that in the class of S_n^{mc} convective cells, J increases with increasing m, and that when $m = 1$ the convergence was doubtful. The class of models S_n^{2c} shown in table 5 yields a *model of minimum dissipation* S_4^{2c}. The value of J for the first mode of S_4^{2c} is less by a factor of 5.4 than for the first mode of S_2^{2c}, and by a factor of 24 relative to the third mode of S_2^{2c}. The ohmic dissipation in S_4^{2c} of 1.8×10^{16} erg s^{-1} is of the order of tidal dissipation in the Bristol channel (Grace 1936), and is only about one-thousandth of the total tidal dissipation in the world oceans. The capacity of some of the large electric power stations in operation is 10^{16} erg s^{-1} (1000 MW). The velocity scale U_0 is only 0.0017 cm s^{-1}. An attempt to adjust the S_4^{2c} model so as to reproduce the observed equatorial dipole components is shown in table 3.

TABLE 4. THE CRITICAL MAGNETIC REYNOLDS NUMBERS R FOR THE HIGHER MODES OF THE S_2^{2c} CONVECTIVE CELL

λ_ν are the roots of (51); N denotes the total number of functions solved for, I the magnetic energy integral (A10) and J the ohmic dissipation integral (A17).

mode ν	N	R	I	J
λ_1	128	99.2	111	1.2×10^4
λ_2	98	36.1	234	2.0×10^4
λ_3	98	29.4	538	5.3×10^4
λ_4	60	28.0	924	1.2×10^5
λ_5	60	27.3	1.4×10^3	2.3×10^5
λ_6	60	26.9	2.0×10^3	4.1×10^5
λ_7	60	26.7	2.9×10^3	7.1×10^5
λ_8	60	26.6	3.9×10^3	1.2×10^6
λ_{10}	60	26.5	6.7×10^3	2.8×10^6
λ_{15}	60	26.4	1.9×10^4	1.5×10^7
λ_{20}	60	26.4	4.2×10^4	5.6×10^7

TABLE 5. SOLUTIONS FOR THE S_n^{2c} CONVECTIVE CELLS

e_M is the magnetic energy density; D denotes the total ohmic dissipation. The ohmic dissipation was computed for an electrical conductivity of $k = 3 \times 10^{-6}$ e.m.u.

model	N	R	I	$10^{-3}J$	e_M/erg cm^{-3}	$10^{-16}D$/erg s^{-1}
S_2^{2c}	128	99.2	111	12.1	11.8	9.9
S_3^{2c}	84	20.5	47	2.5	5.0	2.0
S_4^{2c}	84	22.4	37	2.2	3.9	1.8
S_5^{2c}	84	23.1	48	3.5	5.1	2.8
S_6^{2c}	84	24.0	55	4.8	5.8	3.9
S_7^{2c}	84	24.0	66	6.6	7.0	5.3

7. POLAR AND EQUATORIAL DIPOLE DYNAMOS

The convective models discussed so far were all longitude-dependent through the factor $\cos m\phi$ or $\sin m\phi$ appearing in Y_β of (13). With a view to applications to the Earth's magnetic field, we also limited ourselves to that chain of functions in the solutions of (23) and (24) which starts with the magnetic dipole term $S_1^0(r)$. Still within the latter restriction, let us consider convective cells which have *axial symmetry* and are represented by (20) to (22) with

$$Y_\alpha = P_\alpha(\cos\theta), \quad S_\alpha(r) = (\tfrac{1}{2}\pi\lambda r)^{\frac{1}{2}} J_{\alpha+\frac{1}{2}}(\lambda r) \equiv Q_\alpha(r), \tag{74}$$

where λ is a root of (33). It is found that: (i) the solution $\boldsymbol{H}$ of the dynamo equation (18) is also axisymmetrical; and that (ii) the Bullard–Gellman differential system (23) and (24) separates into two chains, one containing only the poloidal functions S_β of (10) to (12) (but not the T_β), and another chain for the toroidal functions T_β which involves both the S_β and T_β. This means that, if a solution satisfying the boundary conditions exists, the poloidal functions can be solved for by themselves, and the toroidal functions can then be determined from them. Actually, since, as a consequence of the selection rules, the magnetic field is restricted to be axisymmetric, Cowling's theorem forbids such a solution.

This negative result can also be proven directly from the differential equations. The differential equation for the dipole function $S_1^0(r)$ in (23) is

$$r^2\ddot{S}_1^0 - 2S_1^0 = \frac{\mathrm{d}}{\mathrm{d}r}(r^2\dot{S}_1^0 - 2rS_1^0) = R\frac{\mathrm{d}}{\mathrm{d}r}\left\{-\frac{3(\alpha-1)\,\alpha^2(\alpha+1)}{2(2\alpha-1)\,(2\alpha+1)}\,Q_\alpha S_{\alpha-1}^0 + \frac{3\alpha(\alpha+1)^2\,(\alpha+2)}{2(2\alpha+1)\,(2\alpha+3)}\,Q_\alpha S_{\alpha+1}^0\right\}, \tag{75}$$

where $S_{\alpha-1}^0$ are the solutions S_β of (10) to (12) with $\beta = \alpha - 1$, and Q_α is defined in (74). Integrating (75) with respect to r from 0 to 1 we get

$$\dot{S}_1^0(1) - 2S_1^0(1) = 0, \tag{76}$$

since $Q_\alpha(r)$ vanishes both at $r = 0$ and at $r = 1$. Equation (76) is, however, inconsistent with the boundary condition (17), showing that $S_1^0(1) = 0$; i.e. *in the case of axisymmetrical motion there is no solution having a magnetic dipole term oriented along the axis of symmetry of the convective cell.*

There are, however, dipole solutions oriented in the equatorial plane of the convective cell. These arise from chains of equations (23) and (24) whose initial term is not $S_1^0(r)$ but $S_1^{1c}(r)$ or $S_1^{1s}(r)$. In the latter chains, the $S_1^0(r)$ function is missing. This is the class of dynamos discussed by Gubbins (1972). Results for an equatorial dipole dynamo are shown in table 6. The axisymmetric convective cell is represented by (74), with $\alpha = 2$, and the solution starts with the equatorial dipole function $S_1^{1c}(r)$. No solution was found for the first convective mode corresponding to the first root λ_1 of (53), a result also found by Gubbins for his dynamos. The second and third modes yield rapidly converging solutions, since in this chain only the functions $S_n^1(r)$ appear, and the total number N of unknown functions for a given maximum order n of the spherical harmonics is only $2n$.

TABLE 6. SOLUTIONS FOR AN S_2^0 CONVECTIVE CELL STARTING WITH THE EQUATORIAL DIPOLE FUNCTION S_1^{1c}

n denotes the maximum order of spherical harmonics included; N the total number of unknown functions; R the magnetic Reynolds number; I the magnetic energy integral (A10), and J the ohmic dissipation integral (A17).

mode	n	N	R	I	J
λ_1	15	30	no solution		
λ_2	25	50	25.369	129.90	8917
λ_3	25	50	22.088	341.47	30109

The same eigenvalues R would also have been found for the chain starting with the $S_1^{1s}(r)$ equatorial dipole, since the origin of longitude ϕ is arbitrary in an $S_\alpha^0(r)$ convective cell. In addition to the three chains starting with the dipoles $S_1^0(r)$, $S_1^{1c}(r)$ and $S_1^{1s}(r)$, the $S_\alpha^0(r)$ convective cell possesses a fourth independent chain starting with the function $S_2^0(r)$ and containing none of the three dipole functions.

In table 7 we list the functions in the solutions of the dynamo equation (18) which exist for an S_2^{2c} convective cell. The indices give (n, m, c) or (n, m, s) of the functions $S_n^{mc}(r)$ and $S_n^{ms}(r)$ appearing in the expansion (10) to (12) for the solution. There are four independent chains. Chain A represents the solution for the polar dipole, oriented along the two-fold symmetry axis of the S_2^{2c} flow, which was discussed in tables 1, 2, 4 and 5. Chains B and C represent equatorial dipole solutions. We found that in both cases B and C, dynamo solutions exist, as is shown in table 8. The solutions for chains B and C are not identical, because the S_2^{2c} cell does have a longitudinal polarization. Actually the solutions for B and C would be interchanged if the direction of convection were reversed.

TABLE 7. THE INDICES (n, m, c) AND (n, m, s) OF THE FUNCTIONS $S_n^{mc}(r)$ AND $S_n^{ms}(r)$ APPEARING IN THE FOUR INDEPENDENT CHAINS OF THE EXPANSION (10) TO (12) FOR THE SOLUTION OF (18) FOR THE CASE OF AN S_2^{2c} CONVECTIVE CELL

A	B	C	D
10C	11C	11S	20C
22S	21S	21C	22C
30C	31C	31S	32S
32C	33C	33S	40C
42S	41S	41C	42C
44S	43S	43C	44C
...	...	...	...

TABLE 8. EQUATORIAL DIPOLE SOLUTIONS FOR THE CHAINS B AND C OF TABLE 7

chain	mode	N	R	I	$10^{-3}\,J$
B	λ_1	40	34.7	234	17.8
B	λ_2	40	16.7	1087	55.1
B	λ_3	40	15.6	2945	192
C	λ_1	40	17.4	39.5	1.36
C	λ_2	40	15.6	288	16.8
C	λ_3	40	15.3	781	67.6

It is interesting that the dissipation integral $J = 1356$ for the λ_1 solution C is even lower than in the model S_4^{2c} listed in table 5, yielding a rate of total ohmic dissipation of only 1.1×10^{16} erg s^{-1} for an assumed electrical conductivity $k = 3 \times 10^{-6}$ e.m.u. This, however, is not likely to be relevant to the Earth's magnetic field, since it is hard to conceive the origin of a convection whose axis is oriented in the equatorial plane.

The chain D does not have convergent solutions; hence we conclude that there is no dynamo of type D for an S_2^{2c} cell. In the case of an S_3^{2c} cell, there are only three independent chains, with B and C of table 7 merged.

8. REPRESENTATION OF THE CONVECTION

Since most of our discussion is concerned with the S_2^{2c} model, we shall attempt to describe its motion. The velocity components are given by

$$Au_r = (18/r^2)\, Q_2(r) \sin^2\theta \cos 2\phi, \tag{77}$$

$$Au_\theta = (6\dot{Q}_2/r) \sin\theta \cos\theta \cos 2\phi - (6\lambda Q_2/r) \sin\theta \sin 2\phi, \tag{78}$$

and

$$Au_\phi = -(6\dot{Q}_2/r) \sin\theta \sin 2\phi - (6\lambda Q_2/r) \sin\theta \cos\theta \cos 2\phi, \tag{79}$$

where $$Q_2(r) = \left\{\left(\frac{3}{\lambda^2 r^2} - 1\right)\sin \lambda r - \frac{3}{\lambda r}\cos \lambda r\right\}, \tag{80}$$

and the normalization factor A is given by (50). The three-dimensional representation of this flow is cumbersome, but insight can be gained by displaying the flow pattern in the equatorial plane and in the meridional plane passing through $\phi = 0$ and 180°. Figure 8*a* shows the flow in the equatorial plane for the first mode. It can be derived from the stream-function

$$\psi = Q_2^{\frac{2}{3}} \sin 2\phi. \tag{81}$$

The flow is divided into four quadrants, with no fluid crossing the radii $\phi = 0$, 90, 180 and 270°. In the quadrants marked U the u_θ component is upward toward the north, and in those marked D, downward toward the South. It is seen that in the equatorial plane the motion is spiral, the helicity being positive as in a right-handed screw, in accordance with the positive value of λ in (34). Since we assumed the value of λ in (34) to be positive throughout the core, the helicity is positive everywhere. The spiral nature of the flow is shown also in figure 8*b* which gives the stream lines in a meridional plane passing through $\phi = 0$ and 180°. The pattern follows the stream function

$$\psi = Q_2^{\frac{2}{3}} \cos^2 \theta. \tag{82}$$

In this plane also no fluid flows across the four quadrants, the velocity vanishing along the NS axis. The centres of the toruses in figure 8*a* are situated at the points $r_0 = 0.67b$ where $\dot{Q}_2(r_0)$ vanishes, and $\phi = \frac{1}{4}\pi$, $\frac{3}{4}\pi$, $\frac{5}{4}\pi$ and $\frac{7}{4}\pi$. The trajectories of particles starting from these centres lie on the sphere r_0 and have only a u_θ velocity component, the velocity tending to zero as the polar axis is approached.

We have integrated some particle trajectories by solving the equation

$$\frac{\mathrm{d}r}{\mathrm{d}s} = \frac{u_r}{|u|}, \quad \frac{r\,\mathrm{d}\theta}{\mathrm{d}s} = \frac{u_\theta}{|u|}, \quad \frac{r\sin\theta\,\mathrm{d}\phi}{\mathrm{d}s} = \frac{u_\phi}{|u|}, \tag{83}$$

where the velocity components are given by (77) to (79), $|u|$ denotes the absolute value of the velocity, and $\mathrm{d}s$ an element of length along the trajectory. As an example, a particle that started upward in the first quadrant of figure 8*a* came down in the fourth quadrant, up again in the first and then down in the second quadrant.

Figure 9*a* shows the flow pattern in the equatorial plane for the second mode in the S_2^{2c} cell. There is now a circle of radius $r_1 = 0.63b$ where u_r vanishes. For $r < r_1$ the flow pattern is similar to that of figure 8. For $r > r_1$ the flow is reversed. The duplicity of the toruses is also seen in the meridional section shown in figure 9*b*. The flow pattern shown in figure 10*a* for the third mode of the S_2^{2c} model is divided into three zones, with spiral flow of opposite sign in adjacent zones. Similarly, three zones are shown in the meridional section of figure 10*b*.

The stream lines in the polar dipole model S_4^{2c} of minimum dissipation (see table 5) are shown in figure 11. The pattern of flow in the equatorial plane shown in figure 11*a* is similar to that of the S_2^{2c} model. It is derivable from a stream function

$$\psi = Q_4^{\frac{1}{4}} \sin 2\phi, \tag{84}$$

where $Q_4(r)$ is defined in (74). The stream lines in the meridional plane $\phi = 0°$, 180° shown in figure 11*b* are derivable from a stream function

$$\psi = Q_4^{\frac{8}{15}} \cos^{\frac{2}{3}} \theta (7\cos^2\theta - 4). \tag{85}$$

The diagonal lines on which u_ϕ vanishes pass through the angles θ where $\cos^2\theta = \frac{4}{7}$. It is seen that the motion is spiral with positive helicity everywhere.

PHILOSOPHICAL TRANSACTIONS OF THE ROYAL SOCIETY A MATHEMATICAL, PHYSICAL & ENGINEERING SCIENCES

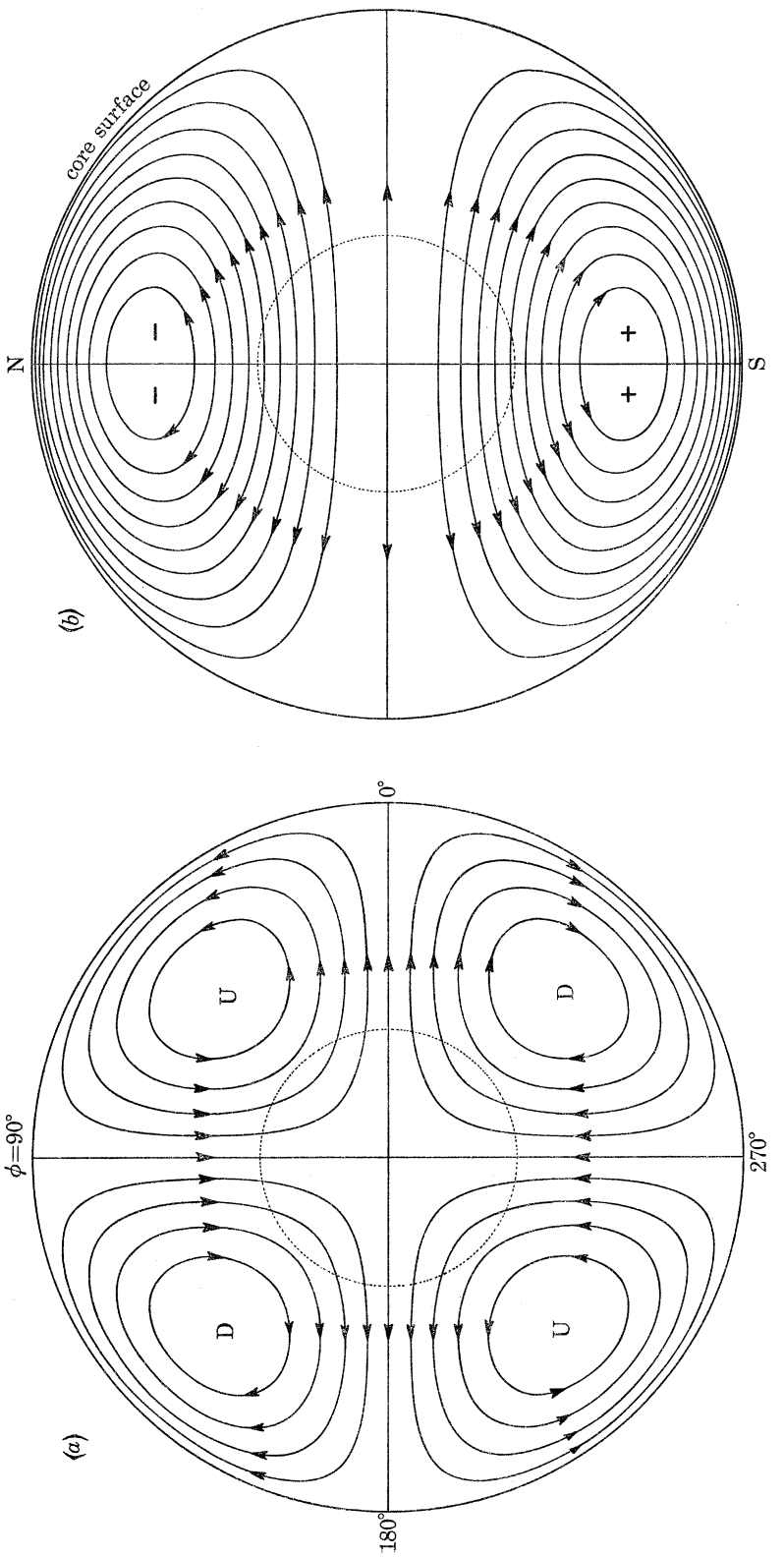

FIGURE 8. (*a*) Stream lines in the equatorial plane. First mode of an S_2^{2c} model. In the quadrants marked U the motion normal to the plane of the equator is northward; in the quadrants marked D, southward. Dots denote boundary of the inner core. (*b*) Stream lines in the meridional plane $\phi = 0°, 180°$. The signs refer to the u_ϕ component.

PHILOSOPHICAL TRANSACTIONS OF THE ROYAL SOCIETY A MATHEMATICAL, PHYSICAL & ENGINEERING SCIENCES

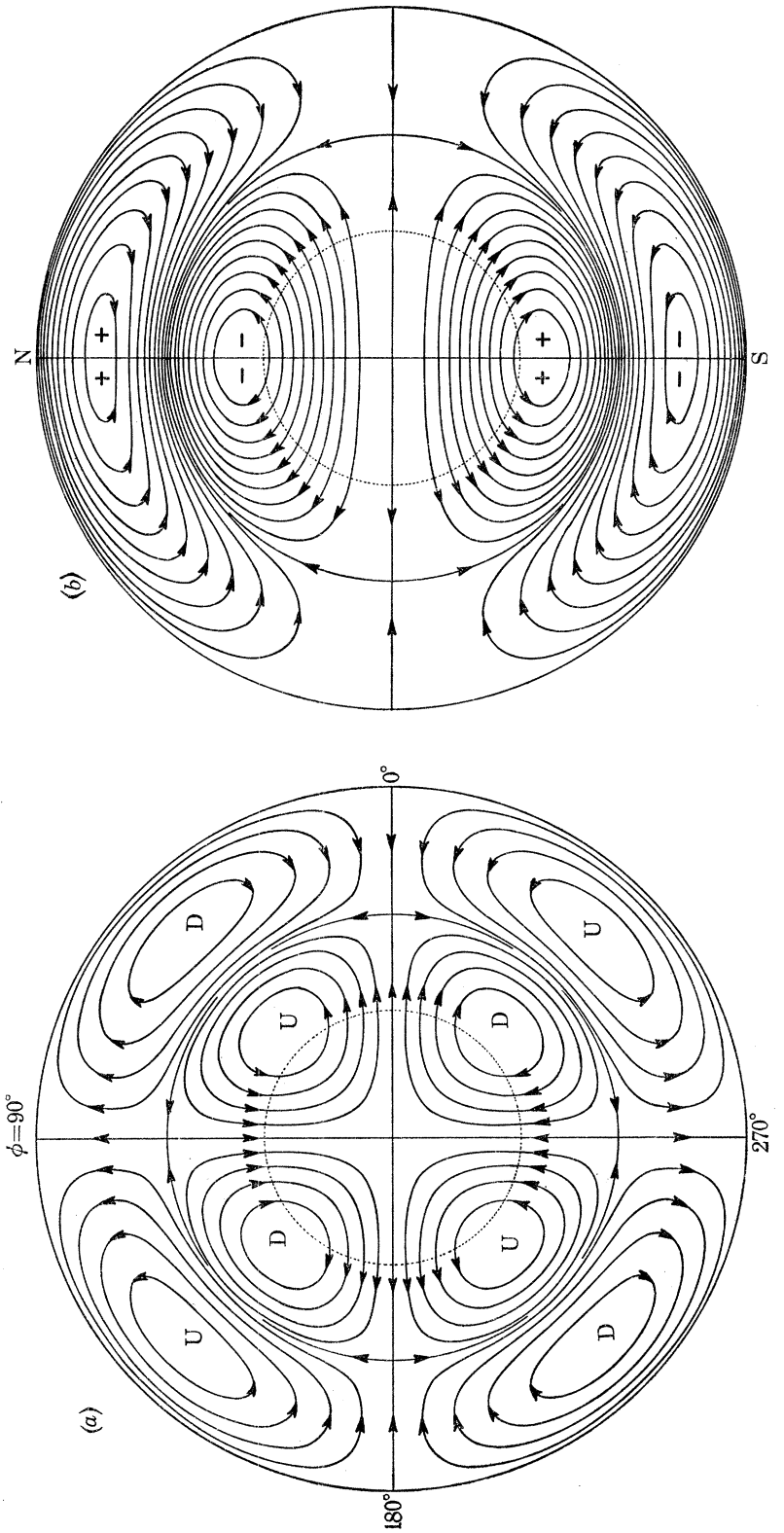

FIGURE 9. (*a*) Stream lines in the equatorial plane for the second mode of the S_2^{2c} model. (*b*) Stream lines in the meridional plane $\phi = 0°, 180°$.

PHILOSOPHICAL TRANSACTIONS OF THE ROYAL SOCIETY A MATHEMATICAL, PHYSICAL & ENGINEERING SCIENCES

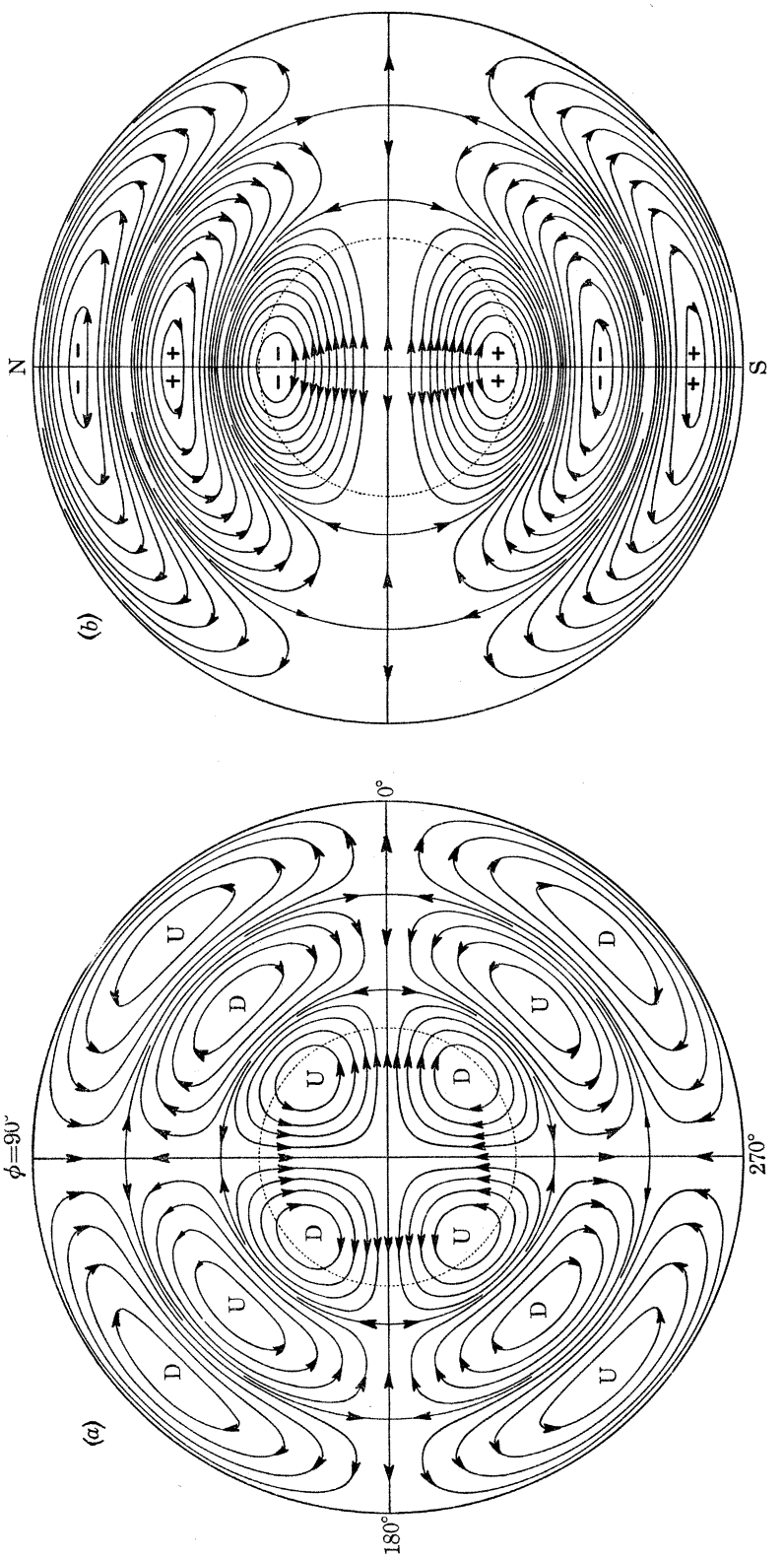

FIGURE 10. (*a*) Stream lines in the equatorial plane for the third mode of the S_2^{2c} model. (*b*) Stream lines in the meridional plane $\phi = 0°, 180°$.

PHILOSOPHICAL TRANSACTIONS OF THE ROYAL SOCIETY A MATHEMATICAL, PHYSICAL & ENGINEERING SCIENCES

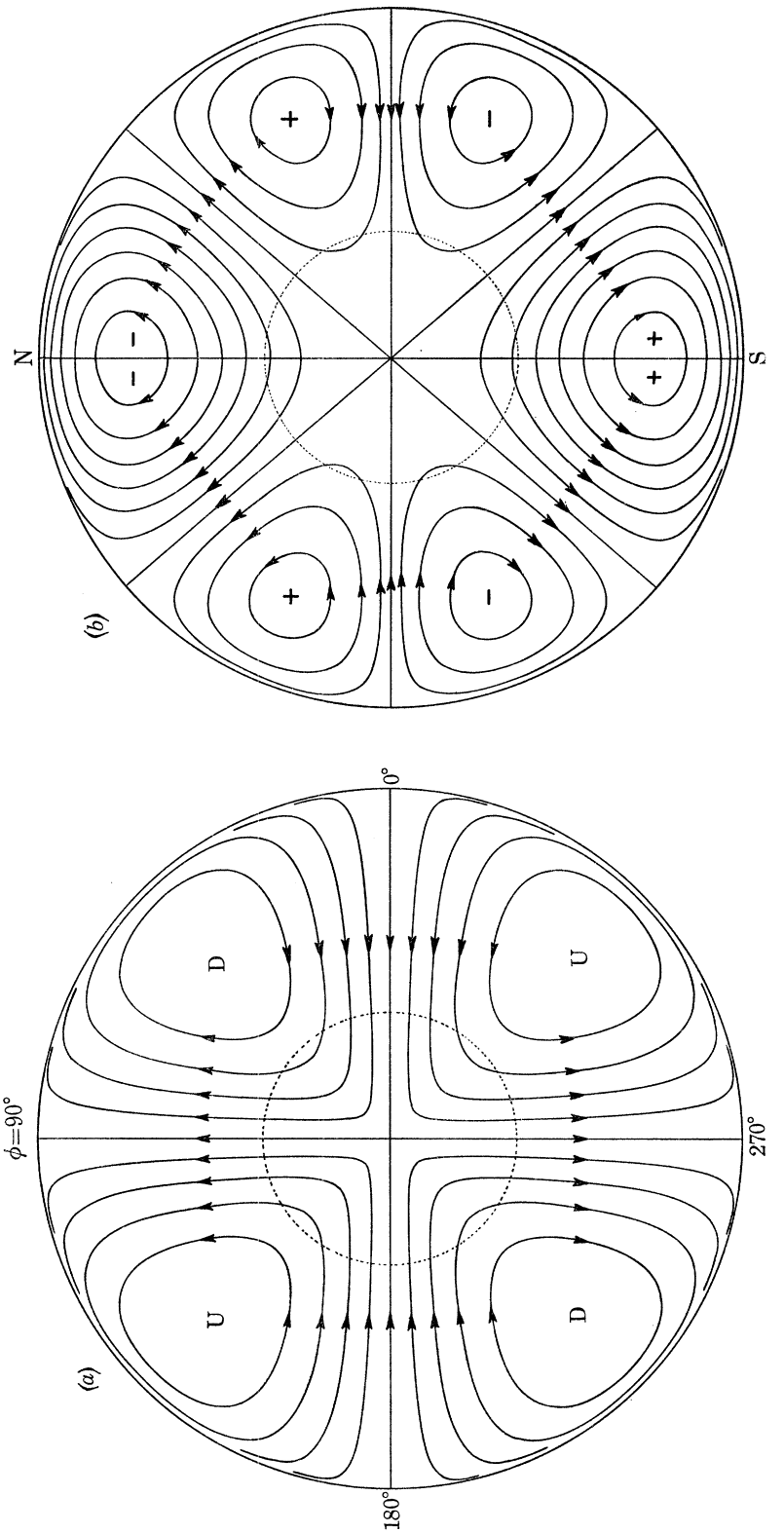

FIGURE 11. (*a*) Stream lines in the equatorial plane for the first mode of the S_4^{2c} model. (*b*) Stream lines in the meridional plane $\phi = 0°, 180°$.

PHILOSOPHICAL TRANSACTIONS OF THE ROYAL SOCIETY A MATHEMATICAL, PHYSICAL & ENGINEERING SCIENCES

9. The internal distribution of the magnetic field

A pictorial representation of the three-dimensional distribution of the magnetic field in the core which is generated by the kinematic dynamos is difficult to make and would not be enlightening. Since, however, the dominant component in the field is the dipole term, which is *axisymmetrical*, we shall describe the mean field $\bar{\boldsymbol{H}}$ (Braginskii 1964) averaged over the longitude ϕ:

$$\bar{\boldsymbol{H}}(r,\theta) = \frac{1}{2\pi}\int_0^{2\pi} \boldsymbol{H}(r,\theta,\phi)\,\mathrm{d}\phi. \tag{86}$$

According to (10) to (12) the mean field $\bar{\boldsymbol{H}}$ is represented by the expansions

$$\bar{H}_r = \sum_n \frac{n(n+1)}{r^2} S_n^0(r)\,P_n(\cos\theta), \quad \bar{H}_\theta = \sum_n \frac{\dot{S}_n^0(r)}{r}\frac{\mathrm{d}P_n}{\mathrm{d}\theta}, \quad \bar{H}_\phi = -\sum_n \frac{T_n^0(r)}{r}\frac{\mathrm{d}P_n}{\mathrm{d}\theta}. \tag{87}$$

In planes passing through the polar axis, the magnetic lines with components $\bar{H}_r$ and $\bar{H}_\theta$ are parallel to the surfaces $\psi_{\bar{H}} =$ constant, where the 'stream function $\psi_{\bar{H}}$' is given by

$$\psi_{\bar{H}} = -\sin\theta \sum_n S_n^0(r)\,\mathrm{d}P_n/\mathrm{d}\theta. \tag{88}$$

Similarly, the mean current $\bar{\boldsymbol{j}}$ has components

$$4\pi b\bar{j}_r = \sum_n \frac{n(n+1)}{r^2} T_n^0(r)\,P_n(\cos\theta), \quad 4\pi b\bar{j}_\theta = \sum_n \frac{\dot{T}_n^0(r)}{r}\frac{\mathrm{d}P_n}{\mathrm{d}\theta}, \quad 4\pi b\bar{j}_\phi = -\sum_n \frac{S_n^{0*}}{r}\frac{\mathrm{d}P_n}{\mathrm{d}\theta}, \tag{89}$$

and in a meridional plane the current is parallel to the lines $\psi_{\bar{j}} =$ constant, with

$$\psi_{\bar{j}} = -\sin\theta \sum_n T_n^0(r)\,\mathrm{d}P_n/\mathrm{d}\theta. \tag{90}$$

The meaning of $\psi_{\bar{H}}$ is that in a cylindrical system of coordinates (ρ, z, ϕ),

$$2\pi\int_0^\rho H_z \rho\,\mathrm{d}\rho = 2\pi[\psi_{\bar{H}}(\rho) - \psi_{\bar{H}}(0)]. \tag{91}$$

Taking $\psi_{\bar{H}} = 0$ on the polar axis, $\psi_{\bar{H}}$ then represents the total magnetic flux crossing a disk of radius ρ and centred on the z axis.

Figure 12 shows the distribution of the magnetic field $\boldsymbol{H}$ and of the electric current $\boldsymbol{j}$ generated in the first mode of the S_2^{2c} model. The magnetic field is given in gauss, and is calibrated in each model so as to give a field of 1.88G at the boundary of the core, as deduced from surface observations by (59). The quantity $\boldsymbol{j}$ is given in units of $(1/4\pi b) = 2.29\times10^{-10}\,\mathrm{A\,cm^{-2}}$. The position of the 'inner core' is indicated by the dotted circle, although in the calculations we assumed liquidity down to the centre. Figure 12*c* shows the distribution of the mean magnetic field $\bar{\boldsymbol{H}}(r,\theta)$ inside the core. The magnetic lines tread a single circle situated in the equatorial plane at $r = 0.81b$ and marked by X. On the circle X lying in the equatorial plane the meridional components of $\bar{\boldsymbol{H}}$ vanish, as envisaged by Cowling (1934) in his original argument. We shall designate this as the *Cowling circle*. Also on X, $\bar{j}_\phi$, shown in figure 12*b*, has a maximum value of -175, the negative sign indicating a current flowing from east to west. Cowling's injunction does not apply because neither $\boldsymbol{H}$ nor $\boldsymbol{j}$ are axisymmetric. The actual distribution of the unaveraged current j_ϕ in the equatorial plane is shown in figure 12*a*. The value of -175 for $\bar{j}_\phi$ on X is the average over the circle marked X in figure 12*a*. Along this circle j_ϕ varies from -100 to -650 at $\phi = 90°, 270°$. The field $\bar{\boldsymbol{H}}(r,\theta)$ in figure 12*c* can be thought of as produced mainly by the intense E to W current belt

centred on the equator in figure 12*b* near the position X. Interestingly, in the region of the 'inner core' $\bar{\boldsymbol{H}}$ is nearly uniform, as in a uniformly magnetized sphere. The averaged currents $\bar{\boldsymbol{j}}$ in meridional planes shown in figure 12*g* are matched both in position and in the proper direction by the associated $\bar{H}_\phi$ shown in figure 12*f*. $\bar{H}_\phi$ is the field that one would expect to be produced by $\boldsymbol{j}$ of figure 12*g*, and its magnitude is of the same order as the components of $\bar{\boldsymbol{H}}$ in meridional planes shown in figure 12*d*. *There is no dominance of the toroidal field over the poloidal*, as was already clear from the respective dipole functions shown in figure 3. At the position X of figure 12*c*, the meridional components of $\bar{\boldsymbol{j}}$ do not vanish, nor does $\bar{H}_\phi$. Note in figure 12*g* that along the NS axis, $\bar{\boldsymbol{j}}$ is southerly in the region of the 'inner core', while in the region of the 'outer core' it is northerly, where it is very intense, as shown in figure 12*h*. The oval-shaped boundary on which $\bar{H}_\phi$ vanishes in figure 12*f* coincides with the line in figure 12*g* where the stream function $\psi_{\bar{j}}$ of (88) vanishes.

Next we wish to examine how the pattern of the internal magnetic field in the dynamo is affected by the order ν of the mode, and by the order n of the spherical harmonic of the convective cell. It is found that, as ν is increased, the region of dynamo action is pulled in toward the centre, while with increasing n the dynamo activity moves towards the surface. This points to a tendency for optimal dynamo action on a scale l which is less than the radius of the core b; it is achieved in the case of large ν by nodes along the radius, and in the case of large n by lateral nodes.

Figure 13 gives the internal field for the third mode of model S_2^{2c}. In comparison with the pattern for the first mode of S_2^{2c} shown in figure 12, we see that the Cowling circle, marked by X, is now at $r = 0.38b$ close to the boundary of the 'inner core'. The mean electric current $\bar{\boldsymbol{j}}_\phi$ shown in figure 13*b* is again concentrated near the equator with a maximum value of -1300 on the Cowling circle X. The field inside the core is everywhere greater than in the first mode, in accordance with the growth of the magnetic energy integral I with increasing order ν of the mode, as shown in table 4. Again, the azimuthal distribution of j_ϕ in the equatorial plane is peaked along longitudes $\phi = 90$ and $270°$, reaching values of -2750 there. The region of the 'inner core' is no longer uniformly magnetized in figure 13*c*, owing to its proximity to the Cowling circle. The electric current $\bar{\boldsymbol{j}}$ along the NS axis in figure 13*g* now suffers six reversals.

Taking the first mode of model S_7^{2s}, we get the pattern of the internal field shown in figure 14. Here we have chosen S_7^{2s} rather than S_7^{2c} in order to preserve symmetry with respect to the NS axis. With increased n the field has withdrawn from the interior of the core towards the surface, as shown in figures 14*d* and 14*h*. The Cowling circle in figure 14*c* is now located at $r = 0.88b$ nearer the surface; there are two of them at $\theta = 49°$ and at $131°$, and this holds also for the $\bar{\boldsymbol{j}}_\phi$ field shown in figure 14*b*.

The S_4^{2c} dynamo is of interest because of its minimum rate of ohmic dissipation. Its internal structure, shown in figure 15, is characterized by a Cowling circle situated at $r = 0.82b$ close to that of the first mode of model S_2^{2c}. $\bar{j}_\phi$ also has a maximum of -40 on the equatorial plane near the Cowling circle. There are, however, in addition, two other maxima at higher latitudes, one of strength -70 and another of $+40$, whose combined effect apparently leaves the equatorial maximum in dominance. The field is weaker everywhere, in accordance with the minimum value of the magnetic energy integral I (table 5). The quantity $\bar{\boldsymbol{j}}$ has two reversals along the NS axis, as in model S_2^{2c}.

10. Effect of the solid inner core

Model S_2^{2c}, third mode, whose internal structure is shown in figure 13, is of questionable relevance, not only because of its relatively high rate of ohmic dissipation (table 4), but also

PHILOSOPHICAL TRANSACTIONS OF THE ROYAL SOCIETY A MATHEMATICAL, PHYSICAL & ENGINEERING SCIENCES

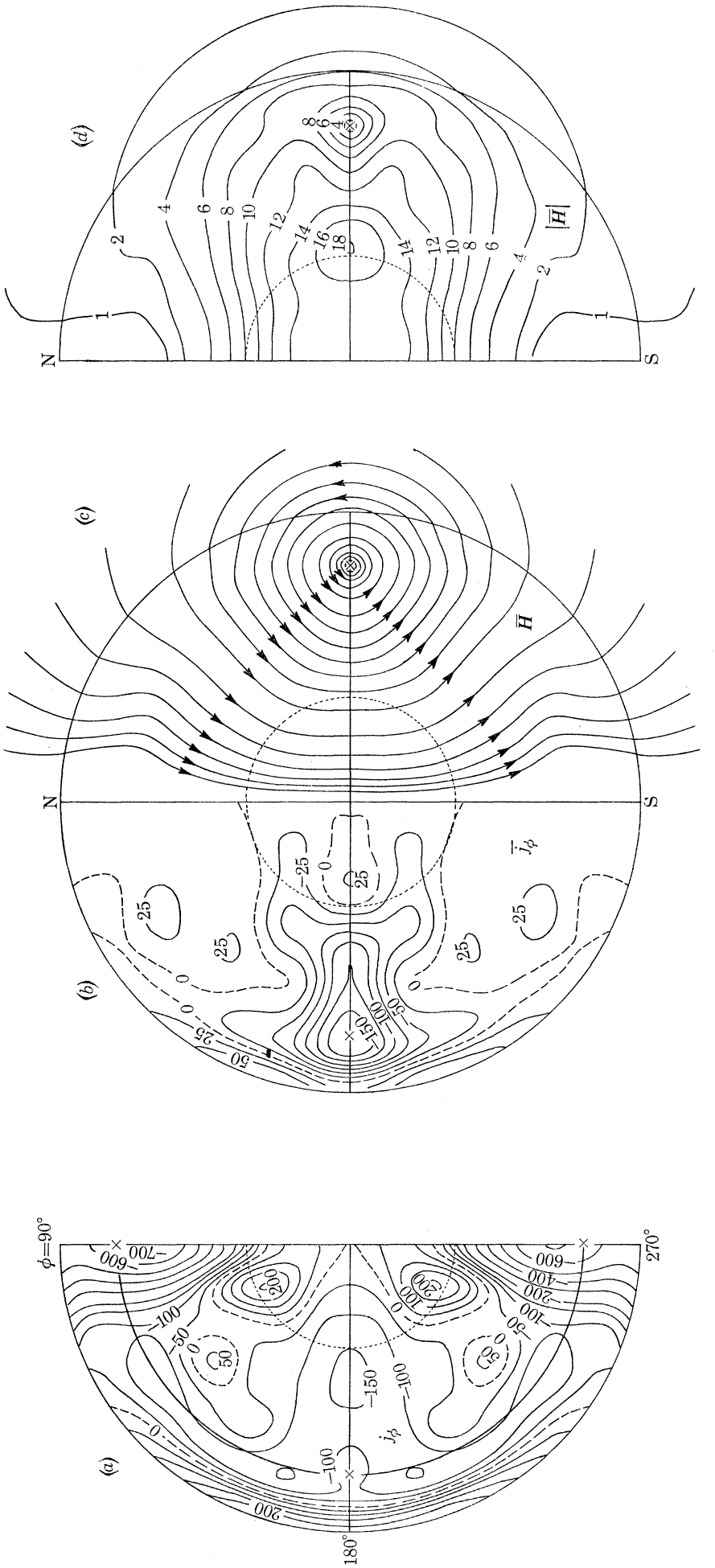

PHILOSOPHICAL TRANSACTIONS OF THE ROYAL SOCIETY A MATHEMATICAL, PHYSICAL & ENGINEERING SCIENCES

PHILOSOPHICAL TRANSACTIONS OF THE ROYAL SOCIETY A MATHEMATICAL, PHYSICAL & ENGINEERING SCIENCES

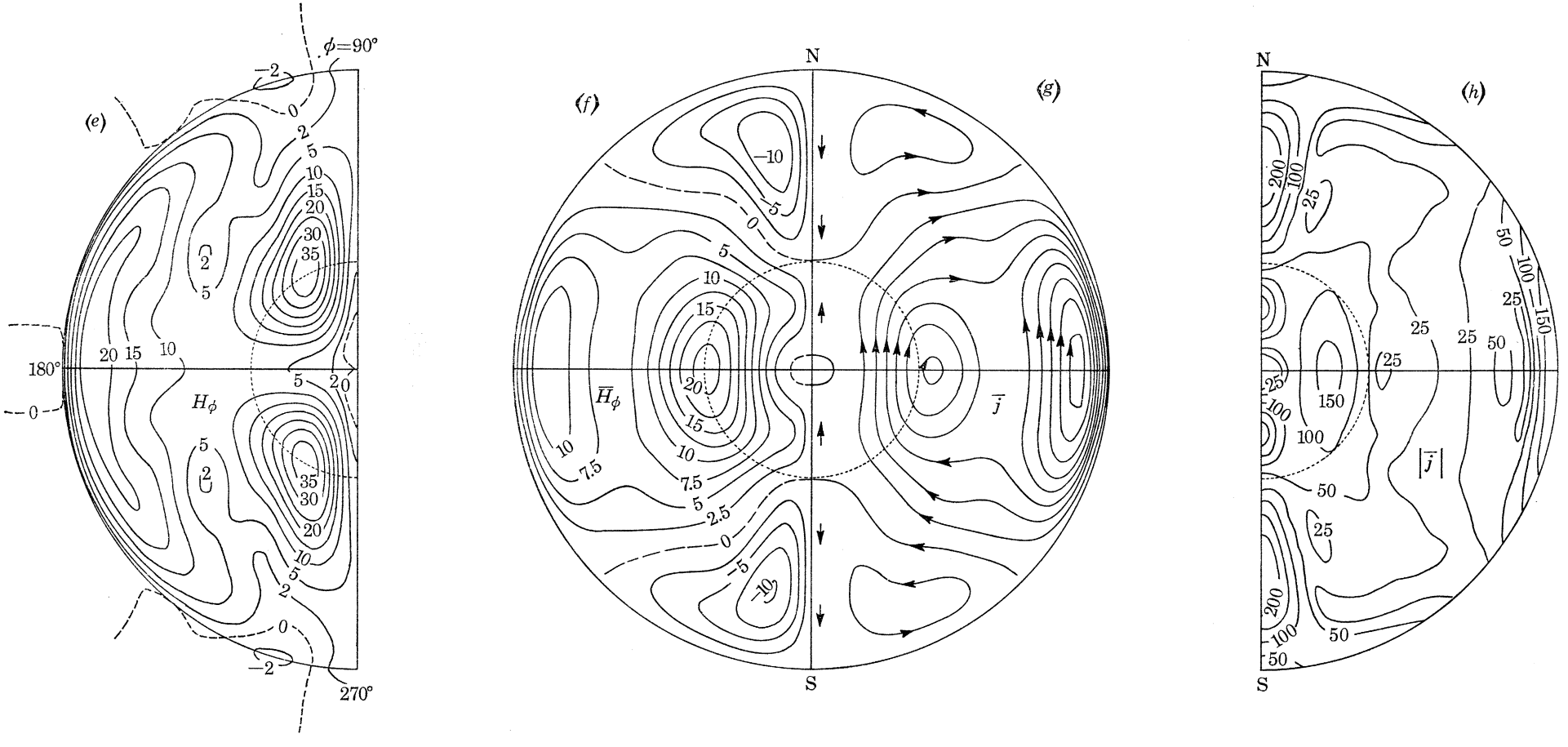

FIGURE 12. Distribution of the magnetic field $\boldsymbol{H}$ and of the electric current $\boldsymbol{j}$ inside the core. First mode of S_2^{2c} model. The bar denotes averaging over longitude ϕ. (*a*) j_ϕ in the equatorial plane. The current is positive from W to E. (*b*), (*c*) and (*d*) $\bar{j}_\phi$, $\bar{\boldsymbol{H}}$ and $|\bar{\boldsymbol{H}}|$ in a meridional plane. (*e*) H_ϕ in the equatorial plane. (*f*), (*g*) and (*h*) $\bar{H}_\phi$, $\bar{\boldsymbol{j}}$ and $|\bar{\boldsymbol{j}}|$ in a meridional plane. $\boldsymbol{H}$ in gauss; $\boldsymbol{j}$ in units of $(1/4\pi b) = 2.3 \times 10^{-10}$ A cm^{-2}; ... boundary of inner core.

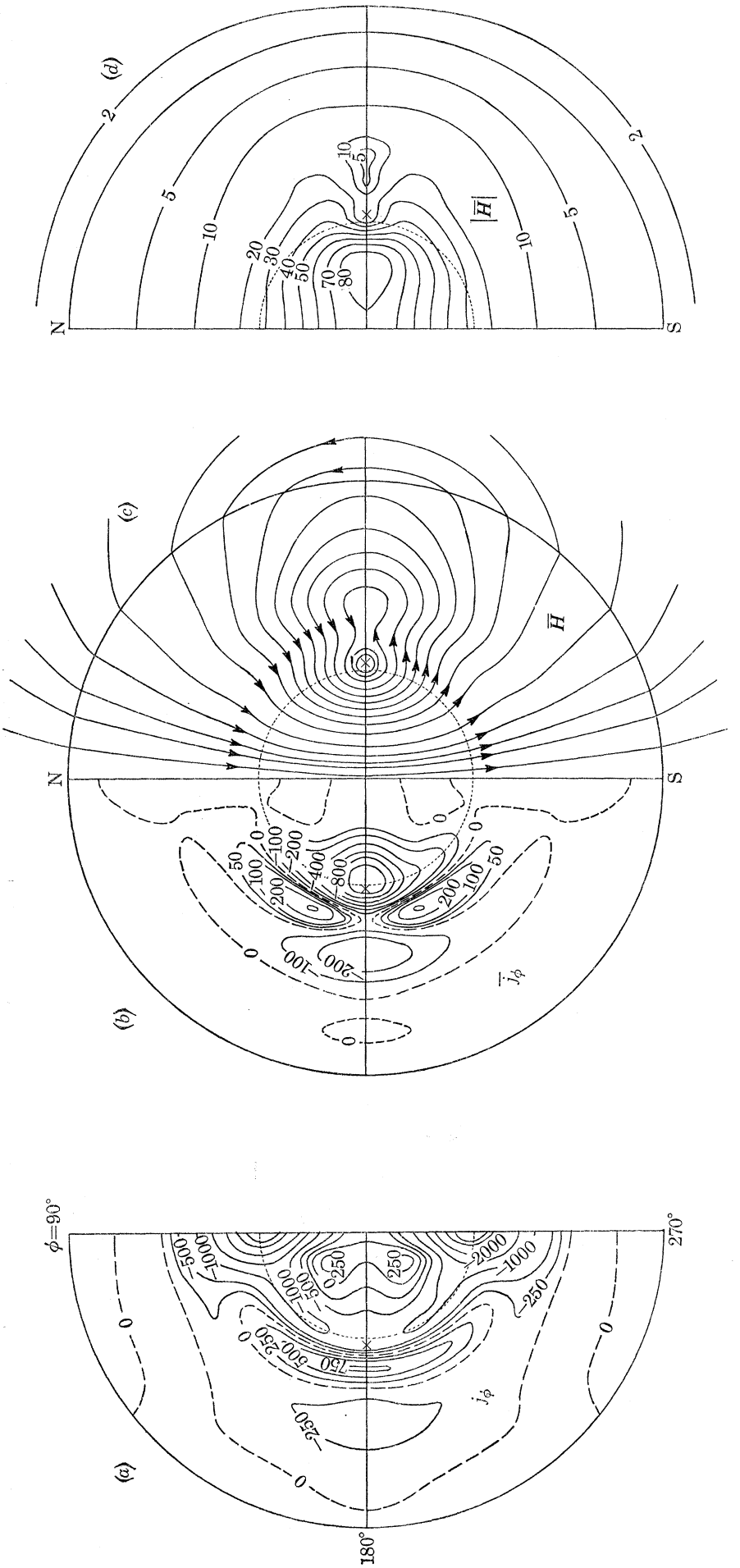

PHILOSOPHICAL TRANSACTIONS OF THE ROYAL SOCIETY A MATHEMATICAL, PHYSICAL & ENGINEERING SCIENCES

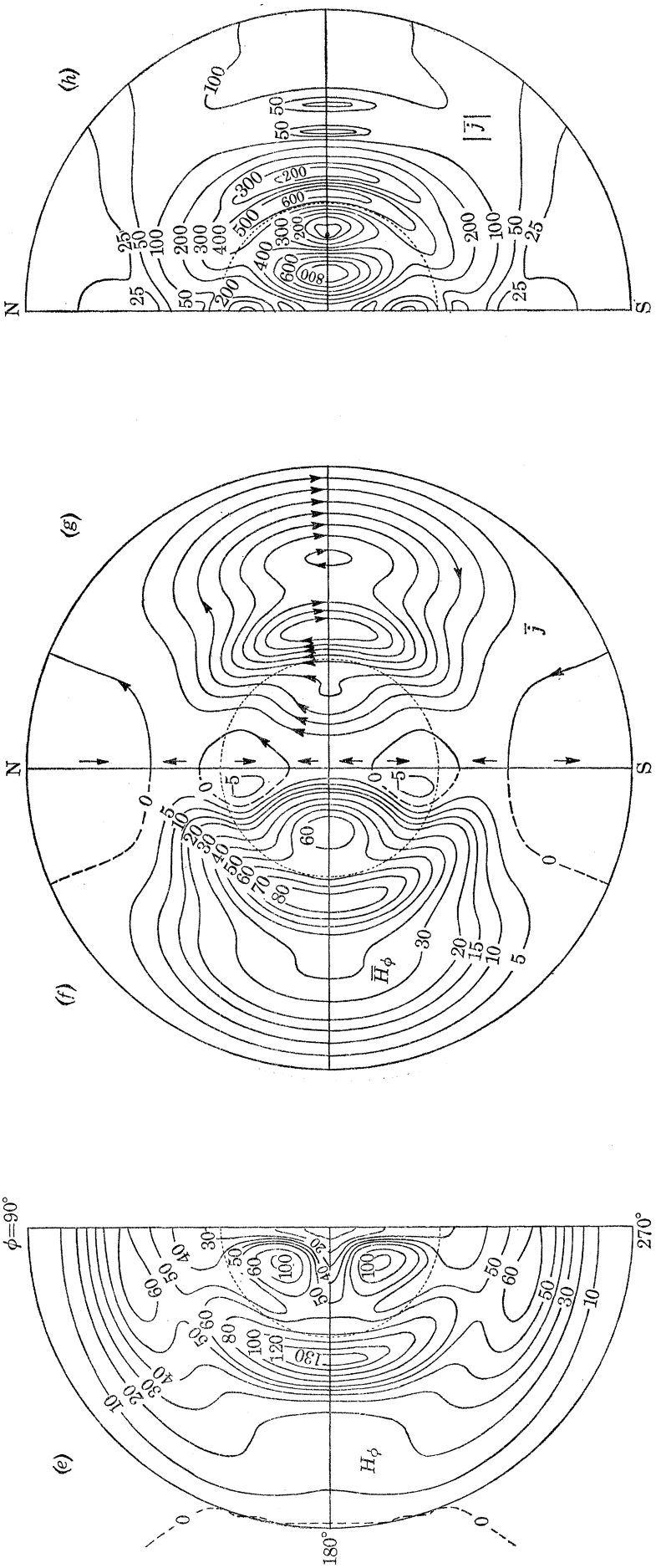

FIGURE 13. Distribution of the magnetic field $\boldsymbol{H}$ and of the electric current $\boldsymbol{j}$ inside the core. Third mode of S_2^{2c} model. See legend of figure 12.

PHILOSOPHICAL TRANSACTIONS OF THE ROYAL SOCIETY A MATHEMATICAL, PHYSICAL & ENGINEERING SCIENCES

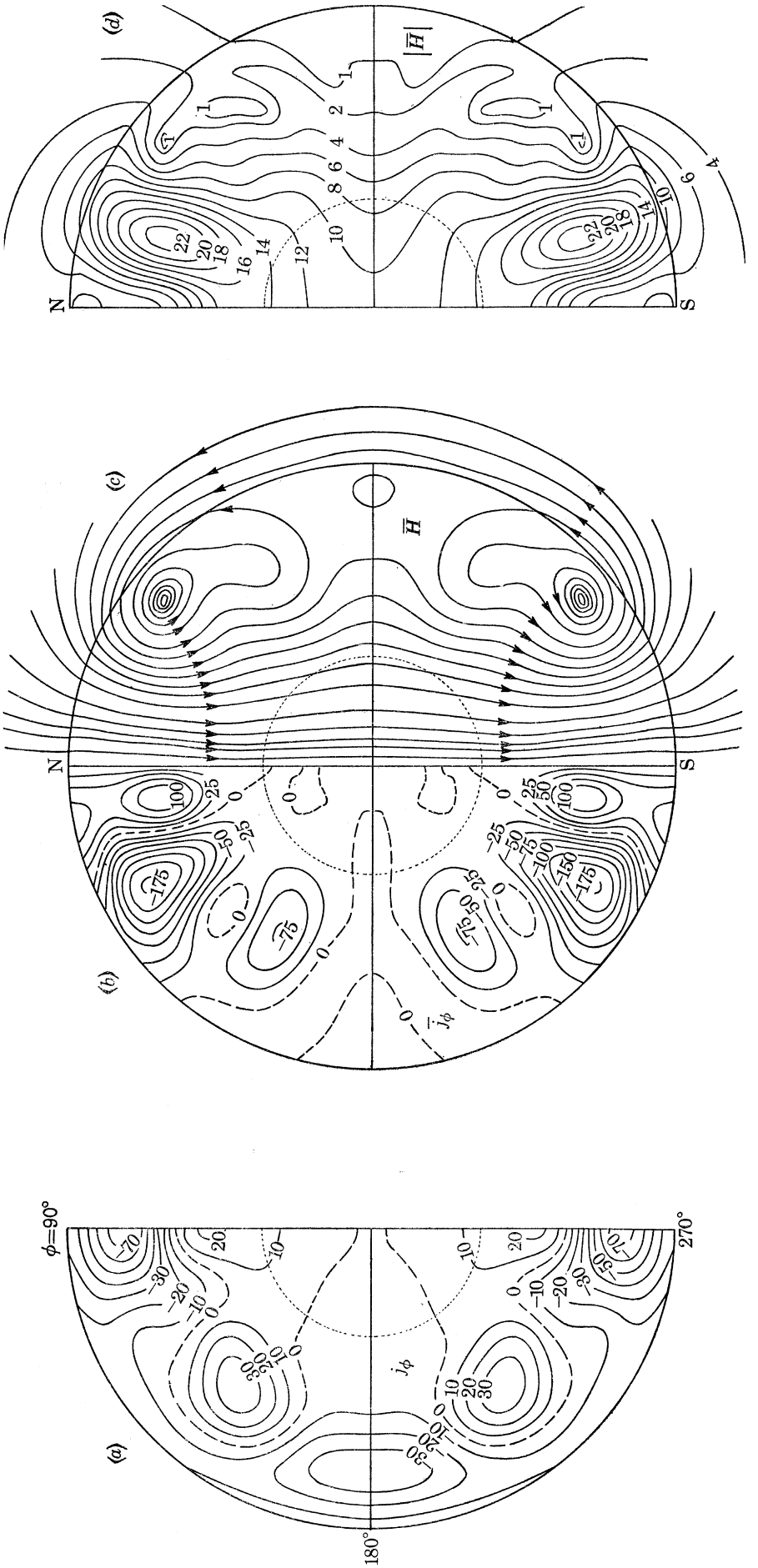

PHILOSOPHICAL TRANSACTIONS OF THE ROYAL SOCIETY A MATHEMATICAL, PHYSICAL & ENGINEERING SCIENCES

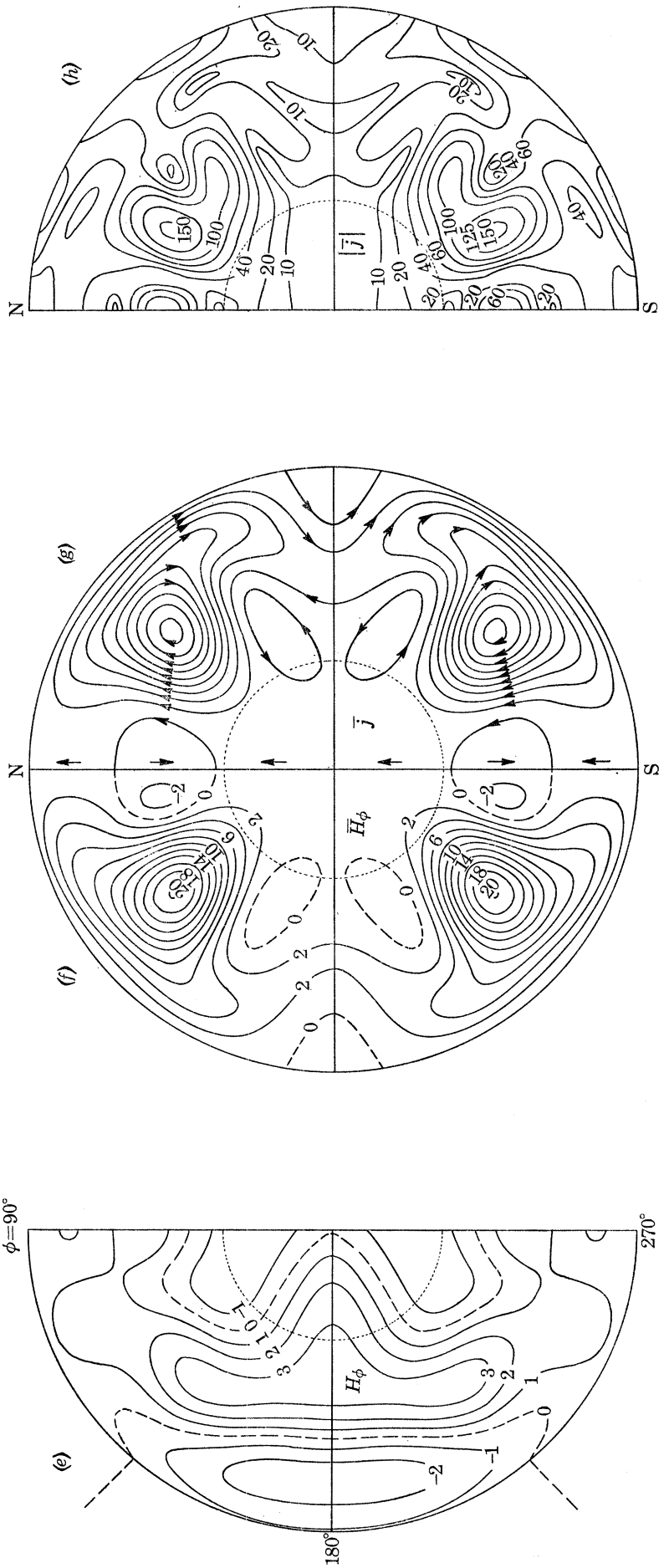

FIGURE 14. Distribution of the magnetic field $\boldsymbol{H}$ and of the electric current $\boldsymbol{j}$ inside the core. First mode of S_7^{2s} model. The bar denotes averaging over longitude ϕ. (*a*) j_ϕ in the equatorial plane. The current is positive from W to E. (*b*), (*c*) and (*d*) $\bar{j}_\phi$, $\bar{\boldsymbol{H}}$ and $|\bar{\boldsymbol{H}}|$ in a meridional plane. (*e*) H_ϕ in the equatorial plane. (*f*), (*g*) and (*h*) $\bar{H}_\phi$, $\bar{\boldsymbol{j}}$ and $|\bar{\boldsymbol{j}}|$ in a meridional plane. $\boldsymbol{H}$ in gauss; $\boldsymbol{j}$ in units of $(1/4\pi b) = 2.3 \times 10^{-10}$ A cm^{-2}; ... boundary of inner core.

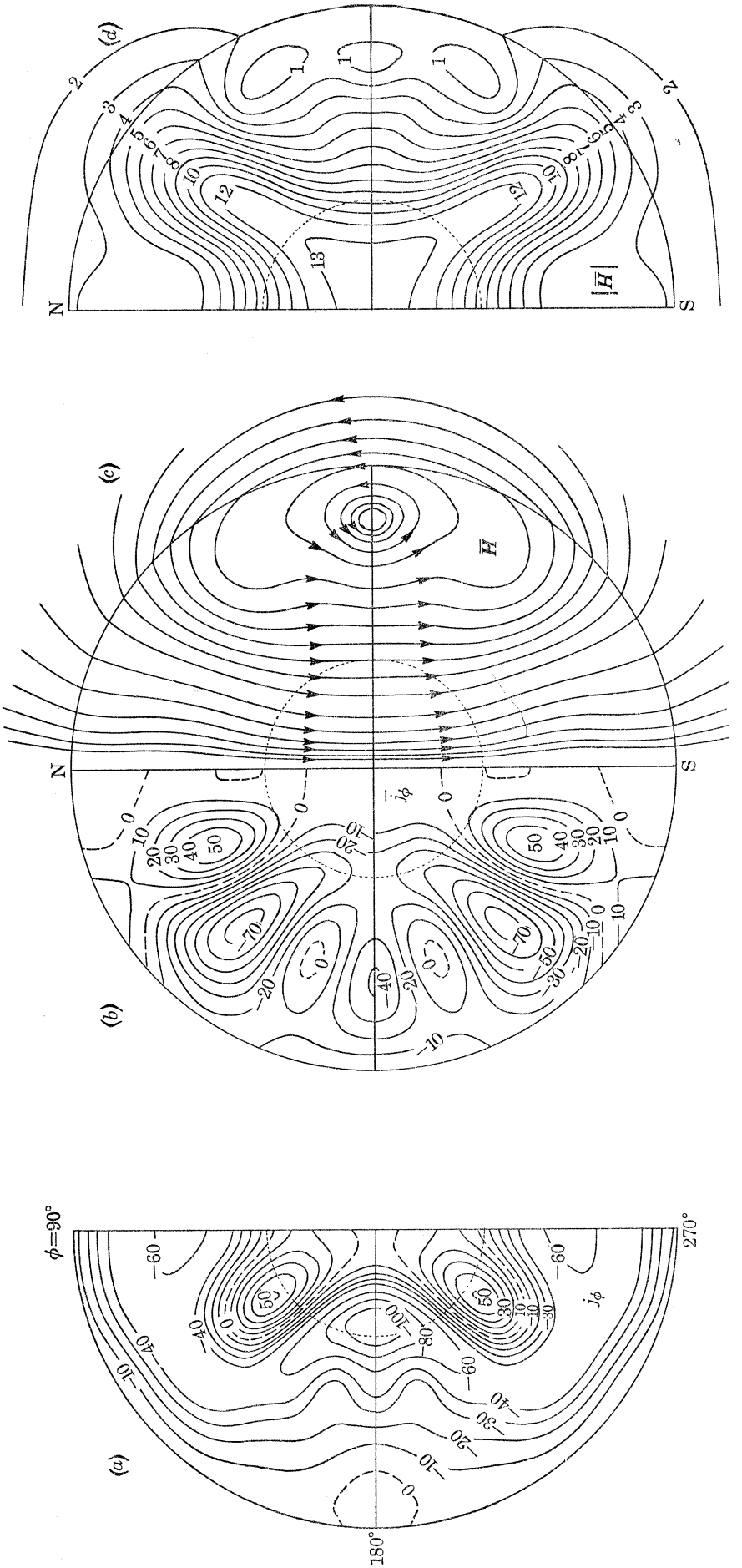

PHILOSOPHICAL TRANSACTIONS OF THE ROYAL SOCIETY A MATHEMATICAL, PHYSICAL & ENGINEERING SCIENCES

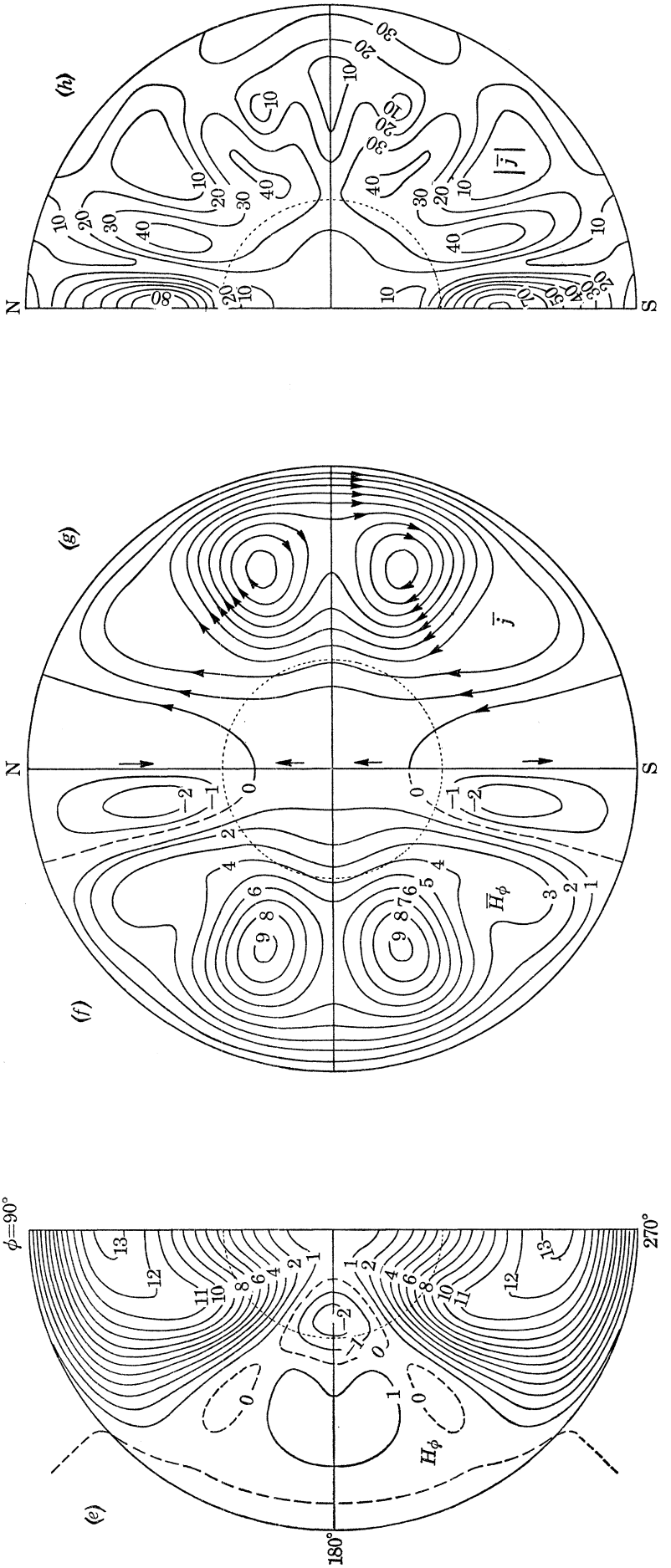

FIGURE 15. Distribution of the magnetic field $\boldsymbol{H}$ and of the electric current $\boldsymbol{j}$ inside the core. First mode of S_1^{2c} model. (See legend of figure 14.)

because its Cowling circle is close to the boundary of the inner core where there is evidence that the material turns solid. We have treated a dynamo with a solid inner core for $r < \omega = 0.36b$. The solutions of (29) have to be modified to provide for a vanishing u_r at $r = \omega$. At $r = \omega$ we also imposed the boundary condition on the solutions S_β and T_β of (18):

$$\omega \dot{S}_\beta(\omega) - (\beta + 1)\, S_\beta(\omega) = 0, \quad T_\beta(\omega) = 0. \tag{92}$$

For the case of the third mode of an S_2^{2c} model we found a convergent solution with eigenvalues and other characteristics which were close to those of the full liquid model.

11. Summary

The purpose of this investigation was to determine whether convergent solutions exist for the stationary kinematic dynamo equations. We follow the Bullard–Gellman (1954) formalism and aim to solve the Bullard–Gellman system of ordinary differential equations with a sufficiently fine integration step h and a high enough order n of spherical harmonics in the expansion, so as to leave little doubt as to the convergence or non-convergence of the solution. In § 2 we treat the class of Bullard–Gellman (1954) dynamos, including the modification introduced by Lilley (1970). Results are given in table 1 for four such kinematic models, and in none of them did the eigenvalue of the magnetic Reynolds number R converge.

Next we treat a class of spherical convective cells characterized by the property of being stationary in a perfect fluid (Pekeris 1972). These are Beltrami flows in which the vorticity vector is parallel and proportional to the velocity vector (equation (34)). They are expressible by the product of a spherical Bessel function of the radius and a single spherical surface harmonic. At the surface of the core the radial component of velocity vanishes, but not the tangential component. The motion is spiral, the sense of rotation coinciding with the sign of λ in equation (34) which was taken to be positive in all of our models. The convection is normalized so that the r.m.s. velocity for the whole core is unity.

In § 4 we treat the kinematic dynamo based on the third mode of the S_2^{2c} convective cell, where the superscript 2c implies a longitudinal factor of $\cos 2\phi$. This flow is represented by equations (47), (48), (77) to (80). The pattern of flow in the equatorial plane is shown in figure 10*a*. For the third mode there are two interior spheres on which u_r vanishes, so that the flow divides into three sets of cells, with opposite directions of motion in neighbouring cells. (See the simpler flow for the first mode in figure 8.) It is seen that in the upgoing cells (U) and in the downgoing cells (D) the sense of spiralling is everywhere positive, as in a right-handed screw. This is also clear in the flow pattern in a meridional plane which is shown in figure 10*b*.

The third mode of the S_2^{2c} model yielded a convergent solution for the dynamo. The results are shown in table 2. As the order of spherical harmonic n was increased to 13, the eigenvalue R approached the asymptotic value of 29.31 by a damped oscillation, which could be represented by equation (54). The degree of convergence of the eigensolutions as n is increased is displayed in figures 1, 2, 4 and 5. A more stringent test of convergence is shown in figures 6 and 7 giving the poloidal and toroidal components of the total magnetic energy. On calibrating the theoretical dipole component so as to fit the observed value of -0.3043G for the magnetic dipole term at the Earth's surface, we find that the average magnetic energy density for this third mode is 57 erg cm^{-3}, and the rate of total ohmic dissipation is 4.3×10^{17} erg s^{-1}. The latter is about two orders of magnitude smaller than the rate of tidal dissipation. The required velocities are only 0.002 cm s^{-1} for

an assumed electrical conductivity $k = 3 \times 10^{-6}$ e.m.u. *The poloidal component of field in the interior is comparable to the toroidal component*, as shown in figure 3. It will be interesting to ascertain how this feature will be affected when the Coriolis force is included.

It is possible to take, instead of S_2^{2c}, a combination of spherical surface harmonics S_2^{mc}, S_2^{ms} which matches not only the observed magnetic dipole term but also the observed harmonics of order one g_1^1 and h_1^1, these being the largest among the non-dipole terms, and representing the deviation of the magnetic axis from the axis of rotation. The result is shown in the line before the last in table 3. *The principal axis of this surface coincides with the axis of the Earth's magnetic dipole.*

We started with the third mode because its convergence was immediately manifest, even though we had to go to a system of 98 unknown functions, involving the solution of a (banded) determinant of order 9800, before it was assured. It was found subsequently that the second mode of the S_2^{2c} model, as well as the first mode, also yielded convergent solutions. In the latter case we had to go to a system of 128 unknown functions ($n = 15$) before the convergence could be established. The results of all the modes of the S_2^{2c} model are shown in table 4. As the order ν of the mode increases, the Reynolds number R approaches an asymptotic value of 26.4. The magnetic energy integral I and the rate of total ohmic dissipation J increase with increasing order ν of the mode, so that the first mode is preferable from an energetic standpoint.

Confining the search to the first mode only, we find (table 5) that the *model S_4^{2c} has a minimum ohmic dissipation* amounting to only 1.8×10^{16} erg s^{-1} or only 1800 MW, which is within the range of existing power stations. This dynamo would require an energy input of only one-thousandth the rate of tidal dissipation, or only one-hundred-thousandth the rate of total heat outflow from the surface of the Earth. The pattern of flow in this model is shown in figure 11. The helicity in the spiral motion is positive throughout, and the scale of the cells is about one-third the radius of the core.

The internal distribution of the magnetic field in the core for the S_4^{2c} model is shown in figure 15. The mean magnetic field $(\bar{H}_r, \bar{H}_\theta)$, averaged over ϕ, in a meridional plane is shown in figure 15*c*. The *Cowling circle* on which $\bar{H}_r$ and $\bar{H}_\theta$ vanish is marked by X and is situated in the equatorial plane at $r = 0.82b$, close to the surface of the core. Within the region of the 'inner core' the mean field is nearly uniform, as in a uniformly magnetized sphere. No violence is done to Cowling's theorem because neither the unaveraged H_r nor H_θ are independent of longitude. The structure of the internal field for other models is shown in figures 12 to 14, and is discussed in § 9.

All of the dynamos discussed so far have as a leading term in their chain of solutions the dipole function $S_1^0(r)$. They produce a magnetic dipole which is oriented along the axis of symmetry of the convective cell, i.e. the polar spherical axis. We designate them as *polar dipole solutions*. When the convective cell is axially symmetric and is represented by a zonal spherical harmonic, it does not possess polar dipole solutions. It can, however, have *equatorial dipole solutions* where the $S_1^0(r)$ term is missing and is replaced by a term S_1^{1c} or S_1^{1s} (Gubbins 1972). Results for equatorial dipole solutions are given in table 8.

12. Conclusions

We have shown that stationary self-exciting dynamos exist for a class of spherical convective cells which would be stationary in a perfect fluid in the absence of rotation and of the magnetic field. Since the Coriolis and magnetic forces are not negligibly small compared to the pressure gradient, we have sought to mitigate the kinematic approximation by seeking such kinematic dynamos in which the rate of ohmic dissipation would be at a minimum. The model S_4^{2c} shown

PHILOSOPHICAL TRANSACTIONS OF THE ROYAL SOCIETY A MATHEMATICAL, PHYSICAL & ENGINEERING SCIENCES

in figures 11 and 15 has a rate of ohmic dissipation of only 1800 MW, which is one-thousandth the rate of tidal dissipation and one-hundred-thousandth the total outflow of heat from the Earth's surface. It is of the order of magnitude of the capacity of existing power plants. The velocities required are of the order of $10^{-3}\,\mathrm{cm\,s^{-1}}$. For an S_2^{2c} model, which has a dissipation greater by a factor of about 5, one can also match the observed equatorial magnetic dipole terms along with the calibrated polar dipole term. This matching is feasible, to a lesser extent, also with the S_4^{2c} model.

The senior author is indebted to the John Simon Guggenheim Memorial Foundation for a Fellowship held during 1972–3. This research was supported by the U.S. Office of Naval Research under Contract N00014-66-C-0080.

Appendix. The total magnetic energy and the rate of joule heat dissipation

The total magnetic energy E_{M} is given by

$$E_{\mathrm{M}} = (b^3/8\pi)\int_0^{2\pi}\mathrm{d}\phi\int_0^{\pi}\sin\theta\,\mathrm{d}\theta\int_0^1 r^2\,(H_r^2+H_\theta^2+H_\phi^2)\,\mathrm{d}r. \tag{A 1}$$

We have from equations (10) to (12)

$$r^2(H_\theta^2+H_\phi^2) = \sum_\beta\sum_\gamma\left\{(\dot S_\beta\dot S_\gamma+T_\beta T_\gamma)\left(\frac{\partial Y_\beta}{\partial\theta}\frac{\partial Y_\gamma}{\partial\theta}+\frac{1}{\sin^2\theta}\frac{\partial Y_\beta}{\partial\phi}\frac{\partial Y_\gamma}{\partial\phi}\right)\right.$$
$$\left.+\,(\dot S_\beta T_\gamma-\dot S_\gamma T_\beta)\frac{1}{\sin\theta}\left(\frac{\partial Y_\beta}{\partial\theta}\frac{\partial Y_\gamma}{\partial\phi}-\frac{\partial Y_\beta}{\partial\phi}\frac{\partial Y_\gamma}{\partial\theta}\right)\right\}. \tag{A 2}$$

Let
$$F_{\alpha\beta\gamma} = \int_0^{2\pi}\mathrm{d}\phi\int_0^{\pi}\sin\theta\,\mathrm{d}\theta Y_\alpha\left[\frac{\partial Y_\beta}{\partial\theta}\frac{\partial Y_\gamma}{\partial\theta}+\frac{1}{\sin^2\theta}\frac{\partial Y_\beta}{\partial\phi}\frac{\partial Y_\gamma}{\partial\phi}\right], \tag{A 3}$$

$$K_{\alpha\beta\gamma} = \int_0^{2\pi}\mathrm{d}\phi\int_0^{\pi}\sin\theta\,\mathrm{d}\theta Y_\alpha Y_\beta Y_\gamma; \tag{A 4}$$

then one can show that

$$F_{\alpha\beta\gamma} = \tfrac{1}{2}[\beta(\beta+1)+\gamma(\gamma+1)-\alpha(\alpha+1)]\,K_{\alpha\beta\gamma}. \tag{A 5}$$

It follows from (A 5) that

$$\int_0^{2\pi}\mathrm{d}\phi\int_0^{\pi}\sin\theta\,\mathrm{d}\theta\left(\frac{\partial Y_\beta}{\partial\theta}\frac{\partial Y_\gamma}{\partial\theta}+\frac{1}{\sin^2\theta}\frac{\partial Y_\beta}{\partial\phi}\frac{\partial Y_\gamma}{\partial\phi}\right) = N_\beta\delta_\beta^\gamma, \tag{A 6}$$

where N_n is defined in (43) and (44). Use was made here of the relation

$$K_{0\beta\gamma} = \int_0^{2\pi}\mathrm{d}\phi\int_0^{\pi}\sin\theta\,\mathrm{d}\theta Y_\beta Y_\gamma = \delta_\beta^\gamma N_\beta/[\beta(\beta+1)]. \tag{A 7}$$

Since

$$\int_0^{2\pi}\mathrm{d}\phi\int_0^{\pi}\mathrm{d}\theta\left[\frac{\partial Y_\beta}{\partial\theta}\frac{\partial Y_\gamma}{\partial\phi}-\frac{\partial Y_\beta}{\partial\phi}\frac{\partial Y_\gamma}{\partial\theta}\right] = 0, \tag{A 8}$$

it follows that

$$E_{\mathrm{M}} = (\tfrac{1}{8}b^3)\,I, \tag{A 9}$$

$$I = \frac{1}{\pi}\sum_\beta N_\beta\int_0^1[\beta(\beta+1)\,(S_\beta/r)^2+\dot S_\beta^2+T_\beta^2]\,\mathrm{d}r. \tag{A 10}$$

The rate of joule heat dissipation D is given, in terms of the current density $\boldsymbol{j}$ and the conductivity k, by

$$D = \int \frac{\boldsymbol{j}^2 \mathrm{d}V}{k}, \tag{A 11}$$

where the integration is to be taken over the volume of the core. Now, by (3) and (10) to (12), we have

$$4\pi b j_r = \sum_\beta \frac{\beta(\beta+1)}{r^2} T_\beta Y_\beta, \tag{A 12}$$

$$4\pi b r j_\theta = \sum_\beta \left(\dot{T}_\beta \frac{\partial Y_\beta}{\partial \theta} + \frac{S^*_\beta}{\sin\theta} \frac{\partial Y_\beta}{\partial \phi} \right), \tag{A 13}$$

$$4\pi b r j_\phi = \sum_\beta \left(\frac{\dot{T}_\beta}{\sin\theta} \frac{\partial Y_\beta}{\partial \phi} - S^*_\beta \frac{\partial Y_\beta}{\partial \theta} \right), \tag{A 14}$$

where

$$S^*_\beta = -\ddot{S}_\beta + \frac{\beta(\beta+1)}{r^2} S_\beta, \tag{A 15}$$

and the factor b stems from the fact that r is non-dimensional, and the curl in (3) introduces a factor of $1/b$. In view of the orthogonality relation (A 6), we get, as for E_{M},

$$D = (b/16\pi k)\, J, \tag{A 16}$$

$$J = \frac{1}{\pi} \sum_\beta N_\beta \int_0^1 [\beta(\beta+1)\,(T_\beta/r)^2 + \dot{T}^2_\beta + S^{*2}_\beta]\, \mathrm{d}r. \tag{A 17}$$

References

Braginskii, S. I. 1964 *Z. eksper. teoret. Fiz.* **47**, 1084 (trans. *Soviet Phys. JETP* **20**, 726).
Bullard, E. C. 1955 *Proc. R. Soc. Lond.* A **233**, 289.
Bullard, E. C. & Gellman, H. 1954 *Phil. Trans. R. Soc. Lond.* A **247**, 213.
Cain, J. C., Daniels, W. E. & Hendricks, S. J. 1965 *J. geophys. Res.* **70**, 3647.
Chandrasekhar, S. & Kendall, P. C. 1957 *Astrophys. J.* **126**, 457.
Cowling, T. G. 1934 *Mon. Not. R. astron. Soc.* **94**, 39.
Elsasser, W. M. 1946 *Phys. Rev.* **69**, 106.
Elsasser, W. M. 1950 *Rev. Mod. Phys.* **22**, 1.
Gibson, R. D. & Roberts, P. H. 1969 In *The application of modern physics to the Earth and planetary interiors* (ed. Runcorn, S.), p. 577. London: Wiley.
Grace, S. F. 1936 *Mon. Not. R. astron. Soc. Geophys. Suppl.* **3**, 388.
Gubbins, D. 1972 *Nature, Lond.* **238**, 119.
Jeffreys, H. 1970 *The Earth*, p. 308. Cambridge University Press.
Larmor, J. 1919 *Br. Ass. Rep. Bournemouth* **159**; *Electr. Rev.* **84**, 412.
Lilley, F. E. M. 1970 *Proc. R. Soc. Lond.* A **316**, 153.
Moffat, H. K. 1969 *J. Fluid Mech.* **35**, 117.
Pekeris, C. L. 1971 *Proc. natn. Acad. Sci., U.S.A.* **68**, 1111.
Pekeris, C. L. 1972 *Proc. natn. Acad. Sci., U.S.A.* **69**, 2460, 3849.
Roberts, P. H. 1972 *Phil. Trans. R. Soc. Lond.* A **272**, 663.

PHILOSOPHICAL TRANSACTIONS OF THE ROYAL SOCIETY A MATHEMATICAL, PHYSICAL & ENGINEERING SCIENCES